



University of
Nottingham

UK | CHINA | MALAYSIA

Functionalisation of an organic-inorganic hybrid polyoxometalate with an organic chromophore

Zimou Feng

20130325

School of Chemistry

Supervised by
Dr Graham Newton

A thesis submitted to the University of Nottingham for the degree of
MRes Chemistry.

March 2020

Abstract

It has been a long-sought scientific target for sustainable chemistry to make effective use of solar energy to drive reactions. Recent research is shining a light on molecular photocatalysts with versatility and tunable properties. Polyoxometalates (POMs) have shown great potential as a result of their appealing photo- and electrochemical properties, as well as their unmatched structural diversity, excellent stability and tunable solubility. In particular, by removing one or more metal centres, POMs can form lacunary derivatives which can be further modified and functionalized. However, the photo-activity of POMs is normally restricted within the UV range and shows little absorption in the visible-light region of the spectrum. On the other hand, perylene diimide (PDI) dyes are a class of cheap and stable organic dyes with strong visible light absorption. It is therefore potentially attractive to tune the inherent properties of POMs with this kind of organic chromophore to form visible-light-driven photocatalysts.

This report describes a modular design approach for a new inorganic-organic hybrid POM which studies the optimization the photocatalytic performance of POM under visible light using a photosensitive ligand system. $[\text{P}_2\text{W}_{17}\text{O}_{61}((\text{P}=\text{O})\text{C}_{26}\text{H}_{12}\text{O}_7\text{N}_2\text{P})_2]$ anion was successfully synthesised and characterised via NMR, Mass Spectrometry, CHN elemental analysis, IR, UV-Vis spectrometry, fluorescence emission and electrochemistry. It was determined that the hybrid POM is successfully obtained and there is photo-driven intramolecular charge transfer from the photoactive organic ligand to the inorganic POM core.

Acknowledgements

I would first like to express my profound gratitude to my supervisor Dr Graham Newton for giving me the chance to start this journey and work in this amazing group. He offered unfailing support and excellent guidance throughout my course. He is always ready to give a talk with enthusiasm and patience, giving me the right direction with distinguished advice on science and helped me fix problems on non-scientific matters. He showed me what a researcher should be and helped me accomplish my own research dream.

I must express my deep gratitude to Dr Jamie Cameron for paying a lot of effort looking after me during this fifteen months. He helped me to chose and improve the project, taught me how to operate reactions and do characterizations, taught me how to solve problems and analyze data. He gave me encouragement and confidence and kept me motivated whenever I was stuck and supported me out of difficult time. He is the first person I would turn to whenever needed.

I would also like to thank Dr Alexander Kibler for sharing with me his ideas and opening the door of photochemistry for me. He spared no effort to help me in times of stress. Thanks to my fellow postgraduate students, particularly Sharad Amin for being my first friend on the first group meeting, and for teaching me NMR and MS. Thanks to Lisa Hampson for teaching me IR and UV-vis, and helping me clean up the mess when I broke things in the lab. Thanks to Luke Francis for helping me with CV and IR, as well as traveling throughout the CNL to recover my data. Thanks to Jack Castle for helping me with report layout and format. Thanks to Neelam Mughal for teaching me analyzing CV data and for her delicious bakings. Thanks to Maggie and Keir for the warm greeting everyday and the laugh brought to the lab. Thanks to the whole Newton group for providing such a pleasant environment to work in.

Finally, I would like to thank my parents for providing me with trust and support throughout my years of study and through the process of researching and writing this thesis.

Colour Scheme

Figures that are not reproduced from literatures and pertain to specific structures adhere to the following scheme:

Tungsten - Light blue

Phosphorus - Pink

Molybdenum - Plum

Vanadium - Blue-gray

Silicon - Orange

Tin - Teal

Sulfur - Gold

Carbon - Grey 50%

Hydrogen - Grey 25%

Oxygen - Red

Nitrogen - Blue

Contents

Abstract	i
Acknowledgements	ii
Colour Scheme	iii
1 Introduction	1
1.1 Polyoxometalates (POMs)	1
1.1.1 Structure and Classification of POMs	2
1.1.2 Synthesis of POMs	5
1.1.3 Wells-Dawson and Lacunary Anions	6
1.2 Electronic and Photocatalytic Properties of POMs	10
1.3 Hybridisation of POMs and Photocatalytic Applications	14
2 Aims	19
3 Results and Discussion	20
3.1 Synthesis and Characterization of Polyoxometalate Starting Materials . . .	20

3.2	Synthesis and Characterization of PMPDI	22
3.3	Synthesis of the PMPDI-POM Hybrid (I and II)	26
3.4	Electro- and Photo-Chemistry of The Hybrid POM	32
4	Conclusion and Further Work	39
5	Experimental	41
5.1	Materials and Instrumentation	41
5.2	Synthesis	42
5.2.1	$K_6[P_2W_{18}O_{62}]$ (P₂W₁₈)	42
5.2.2	α - $K_{10}[P_2W_{17}O_{61}] \cdot 20 H_2O$ (P₂W₁₇)	43
5.2.3	$C_{26}H_{16}O_{10}P_2N_2$ (PMPDI)	44
5.2.4	$[C_2H_6N]_6H_4[P_2W_{17}O_{61}((P=O)C_{26}H_{12}O_7N_2P)_2] \cdot 14 H_2O$ (I)	45
5.2.5	$[C_{16}H_{36}N]_{10}[P_2W_{17}O_{61}((P=O)C_{26}H_{12}O_7N_2P)_2]$ (II)	45
5.3	Benzyl Alcohol Photo-Oxidation	46
	Bibliography	46

1 Introduction

1.1 Polyoxometalates (POMs)

Polyoxometalates (POMs) are an intriguing class of discrete metal-oxide clusters which are formed from early transition metal (Figure 1.1) cations in their highest oxidation states. The clusters are bridged to each other or linked by oxo ligands, and oxoanion heteroatoms often act as template of POMs structures. POMs are normally formed by oxoanions of transition metals (TMs) self assembling to each other or condensing in an acidic environment. Common transition-metals forming POMs include $V^{IV,V}$, Mo^{VI} and W^{VI} ^[1] and template oxoanions include PO_4^{3-} , SiO_4^{3-} and SO_4^{2-} ^[2,3]. POMs have diverse structures, most of them have impressive photoactivity and electronic properties^[4].

	scandium 21 Sc 44.956	titanium 22 Ti 47.867	vanadium 23 V 50.942	chromium 24 Cr 51.996	manganese 25 Mn 54.938	iron 26 Fe 55.845	cobalt 27 Co 58.933	nickel 28 Ni 58.693
	yttrium 39 Y 88.906	zirconium 40 Zr 91.224	niobium 41 Nb 92.906	molybdenum 42 Mo 95.94	technetium 43 Tc [98]	ruthenium 44 Ru 101.07	rhodium 45 Rh 102.91	palladium 46 Pd 106.42
57-70 *	lutetium 71 Lu 174.97	hafnium 72 Hf 178.49	tantalum 73 Ta 180.95	tungsten 74 W 183.84	rhenium 75 Re 186.21	osmium 76 Os 190.23	iridium 77 Ir 192.22	platinum 78 Pt 195.08
89-102 * *	lawrencium 103 Lr	rutherfordium 104 Rf	dubnium 105 Db	seaborgium 106 Sg	bohrium 107 Bh	hassium 108 Hs	meitnerium 109 Mt	ununnium 110 Uun

Figure 1.1: Common metals that can form POMs

POMs occupy a unique position somewhere between meso-scale and nano-scale molecular materials. In particular, they are highly functionalisable through a range of synthetic approaches, allowing the properties of the resultant cluster species to be finely tuned by

controlled modification of the structure and composition of the metal-oxide shell. An especially attractive approach involves the replacement of one or more metal centres with organic moieties, yielding organic-inorganic hybrid polyoxometalates species which have been explored as new photoactive materials for photo- and electro-catalysis^[5,6]. These species are of particular interest because it has been shown that organic functionalisation is a powerful means to both directly tune the electronic structure of the POM^[7], whilst adding additional function or properties through the inclusion of select organic functionalities.

1.1.1 Structure and Classification of POMs

Although there is a large amount of POM structures with various shapes and sizes, they can be defined by a set of quite straightforward structural concepts. Despite their large sizes and complicated composition, POMs are mostly assembled by individual metal oxide polyhedra units. Each unit is composed of a metal atom coordinated to 4 to 7 oxo-ligands, and can be expressed as $[\text{MO}_x]$ where $x = 4 - 7$ (6 is the most common in POM structures) (Figure 1.2 left). These addenda metal ions in the centre are usually early transition metals of groups V and VI (such as V, W, Mo) in their highest oxidation states (the electronic configuration is either d^0 or d^1). The oxo-ligands act as bridging atoms between metals and reinforce the structures^[8]. The M–O oxo-groups which can link anywhere

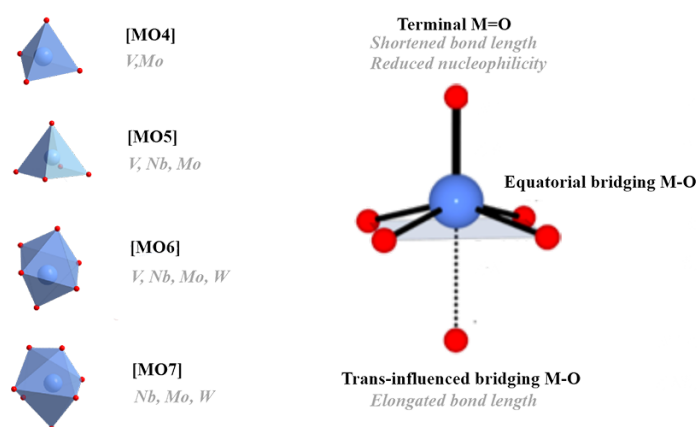


Figure 1.2: Left: Possible $[\text{MO}_x]$ building blocks in POM structures. Right: Main structural features of the most common $[\text{MO}_6]$ polyhedra.

between two to six addenda atoms lead to the multiple metal oxide structures. The formation of terminal M=O bonds acts as the key to the stability of clusters in many kinds of octahedral configuration POMs by weakening the opposite vertex oxygen atom sharing its orbital, resulting in strong thermodynamic counteraction and a displacement from standard octahedron (Figure 1.2 right). The terminal M=O are shortened and less nucleophilic and do not tend to form bonds with metal atoms, whilst the bridging M–O are more nucleophilic which tend to connect the positively charged addenda atoms and heteroatoms. Further condensation reactions of single units may lead to polymeric metal oxides, but these typically acid mediated reaction are avoided by basicity of the surface terminal M=O, as the result of high polarisation of addenda metal towards oxo-ligands.

Another reason of the structural variety of POMs is the formation modes during acid-mediated condensation of single $[MO_x]$ polyhedra. There are three ways distinguished by the number of oxo-ligands shared by two octahedral units to connect each unit during polymerisation : corner sharing, edge sharing and face sharing (Figure 1.3). These motifs are often combined in single anion structures, but the construction is limited by the Lipscomb Principle^[9] which stipulates that no more than two unshared terminal oxo-ligands should be seen in any polyhedra. Based on this rule that is applicable to all POM structures, clusters can generally be classified into three types. The POMs only possessing octahedra with one M=O are type I POMs while type II POMs are those only containing octahedra with two terminal cis-oxo ligands, and type III POMs possess both kinds of octahedra^[10] (Figure 1.4). Normally type I and III POMs show reversible redox chemistry^[11]. Whilst type II POMs are unable to be reduced easily^[12].

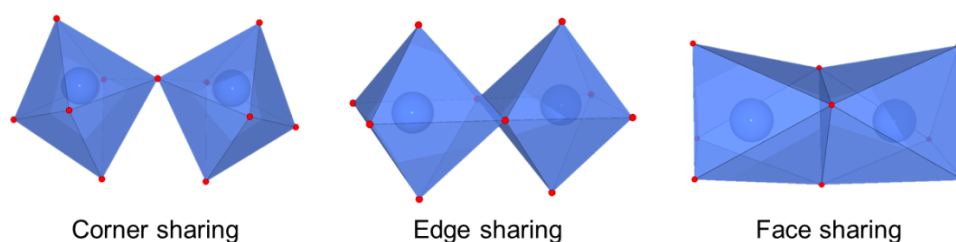


Figure 1.3: Binding modes of polyhedral units

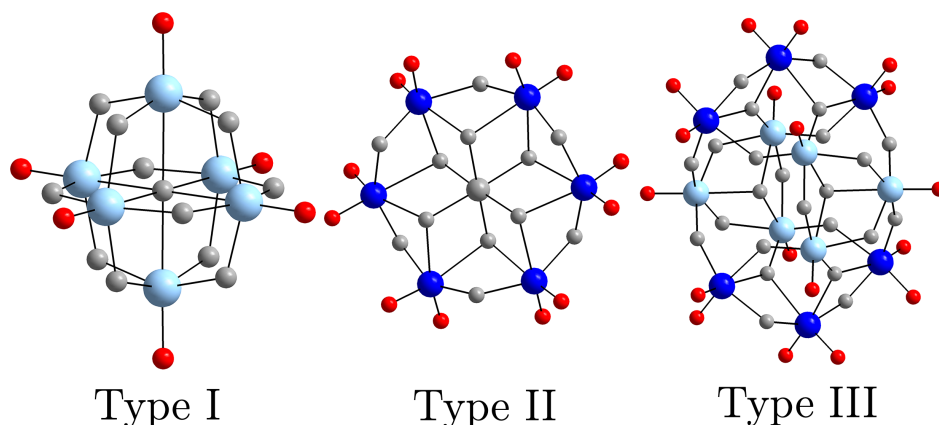


Figure 1.4: Three types of POMs

When POM structure is discussed from the point of view of individual metal oxide polyhedra unit, a final important element is heteroatoms which are cationic guests acting as templating atoms inside the POM core, which are normally p-block or d-block elements. Due to the trans-effect, the inward facing M=O bonds are weakened by the strongly polarised outward facing terminal oxo-ligands, resulting in space inside POM clusters for a large range of sizes of heteroatoms. The POMs which contain heteroatoms are defined as heteropolyoxometalates while isopolyoxometalates refers to those that do not. Some isopolyoxometalates possess a μ_6 oxo-ligand instead as templating atom (Figure 1.5)^[13]. The shape and charge affected by various heteroatoms lead to numerous structures and properties in POMs.

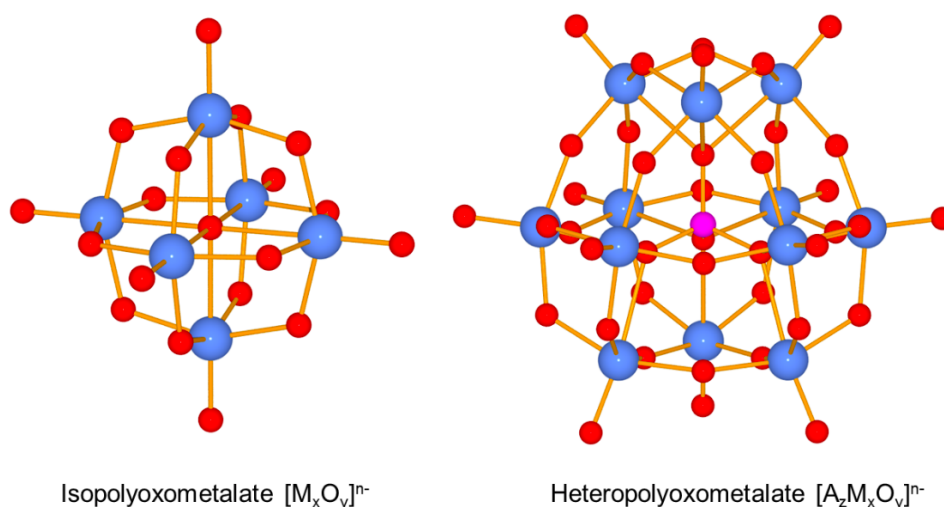


Figure 1.5: Binding modes of polyhedral units

There are lots of compounds with various constitutions, sizes and properties which could be classified as POMs since it is a broad concept (Figure 1.6). However materials defined as POMs can be categorised by several criterions. The most concise factor is the addenda metal^[8], according to which there are polyoxotungstates, polyoxomolybdates, polyoxovanadates and so on^[14]. These also show some general trends in redox properties (redox potential $V > Mo > W$) and kinetic stability ($W > Mo > V$). The second classification depends on whether there is a template heteroatom or not as mentioned in Section 1.1.1. Heteropolyoxometalates are multiple in quantity and generally show more attractive properties than isopolyoxometalates^[8]. The final way of POM distinction is determined by if the structure is complete or one or more addenda metal is removed, giving the concept of plenary and lacunary POMs.

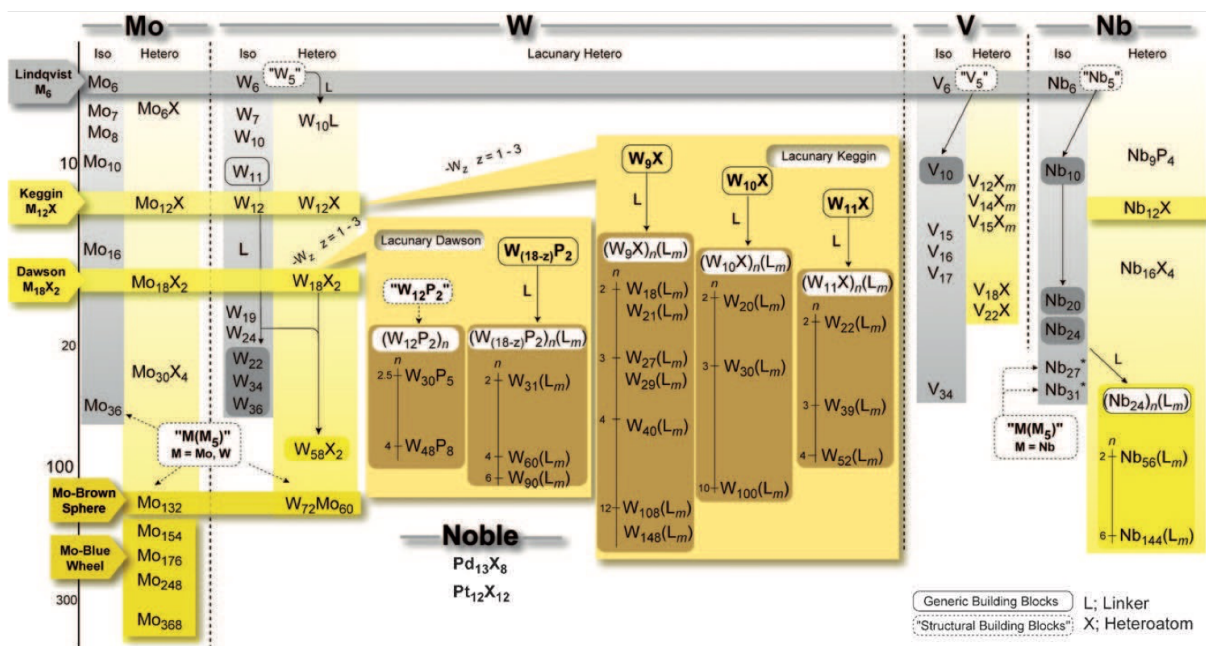


Figure 1.6: Schematic showing the classification of POMs. Figure reproduced from reference 2.

1.1.2 Synthesis of POMs

Typically, POM clusters are formed in aqueous solution through acid-mediated self-assembly of individual metal oxyanions (Figure 1.7). Firstly, the tetrahedral $[MO_4]$ unit is introduced by water soluble oxometalate salts like Na_2WO_4 and Na_2MoO_4 , and the

coordination shell is expanded to form metal hydroxide complexes $[\text{MO}_x(\text{OH})_y]$, which are subsequently acidified to protonated single oxometalate units that can then undergo a series of polycondensation reactions leading to the formation of discrete anionic clusters. Subsequently, suitable counter ions can be used to make the POM precipitate and appropriate purifying approaches (decided by the particular synthetic method) are applied.

Numerous synthetic factors can affect the self-assembly processes, including pH, temperature, cation, type and proportion of heteroatoms^[15]. Selection of solvent may also have influence on the reaction. Apart from water, polar organic solvents can also be adopted^[16,17,18]. Although there are some reproducible well-established structures, it can be a great challenge to speciate new polyoxometalate species due to poor understanding of self-assembly, making it unrealistic to control these processes by simply changing conditions or combine the synthetic variables^[19]. Therefore POM chemistry depends largely on empirical foundations.

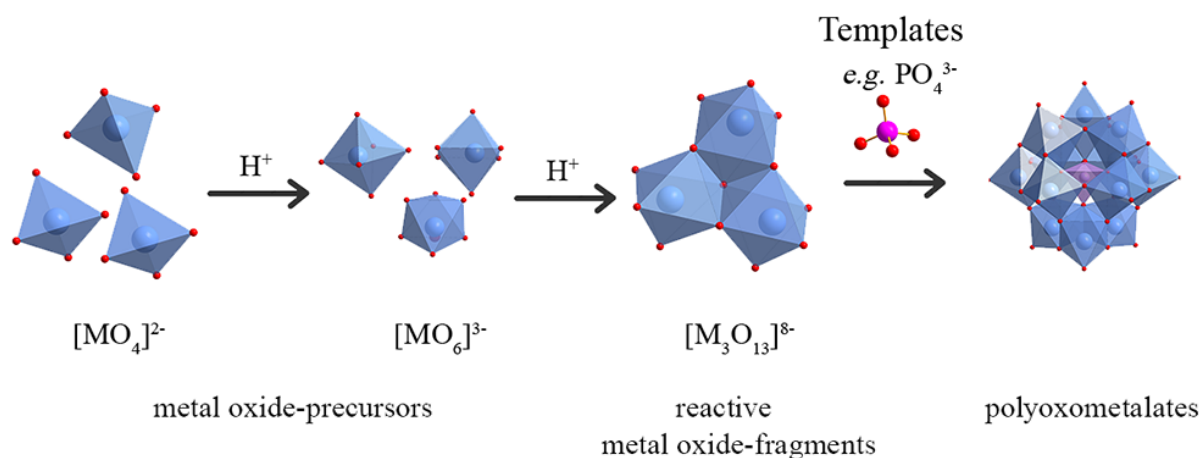


Figure 1.7: General synthesis pathway of POM clusters from monomeric metal oxalate units to polyoxometalates, adapted from reference 20.

1.1.3 Wells-Dawson and Lacunary Anions

Despite the enormous scope of possible POM structures, they can be described according to several common structures recognised as archetypal polyoxometalates building blocks^[2] (Figure 1.8). The archetypal clusters appear commonly as recognisable moieties owing to

their structural stability. Usually they are referred to by the name of who first reported the structure, such as the Lindqvist structure^[21], the Anderson-Evans structure^[22], the Keggin structure^[23] and the Wells-Dawson structure^[24].

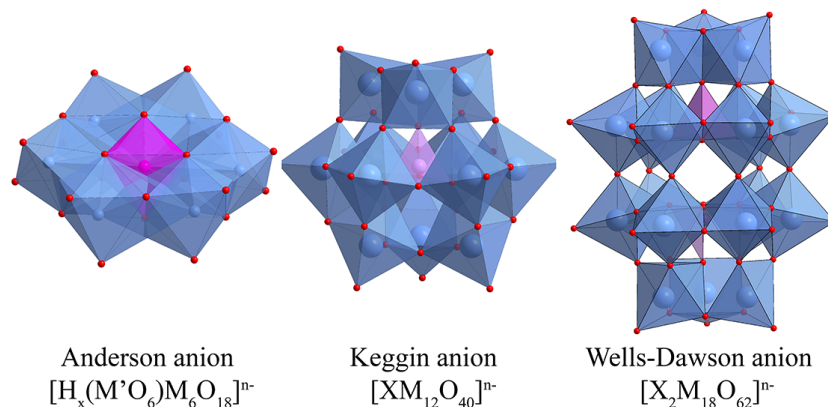


Figure 1.8: Three archetypal polyoxometalates structures

The Wells-Dawson is one of the most common archetypal anions. It was first proposed by Wells in 1945 and identified in 1953 by Dawson via single crystal X-ray diffraction^[25]. With the general formula $[X_2M_{18}O_{62}]^{n-}$ (X represents the heteroatom)^[26], the classic Dawson cluster structure is viewed as two corner-sharing tri-lacunary α -Keggin clusters $A-[XM_9O_{34}]^{n-}$ half units. Each unit consists of a belt of six $[MO_6]$ and a cap of a M_3O_{13} group sharing oxygen atoms of an $[XO_4]$ tetrahedron. Each $[MO_6]$ in belt region is connected to four other $[MO_6]$ by one edge sharing and three corner sharing (Figure 1.9), resulting in significantly reduced metal-metal coulombic repulsions, leading to the excellent thermodynamical stability of Dawson anions.

There are two metal environments in Dawson clusters, six in cap environments and twelve in belt environments. Whilst 62 oxygen atoms can be assigned to eight environments, O_a atoms connect the core heteroatoms to metals, O_b atoms act as bridges between metal atoms and O_c atoms are terminal atoms located on the metals. The heteroatom was linked to the cap metals by two O_{a1} oxygen atoms and linked to belt metals by six O_{a2} atoms, while six O_{b1} atoms bridge the cap metals and 12 O_{b2} atoms link the cap metals to belt metals, twelve O_{b3} connect belt metals inside single belt and six O_{b4} atoms between two belts. Six O_{c1} atoms are located on cap metals and twelve O_{c2} on belt metals.

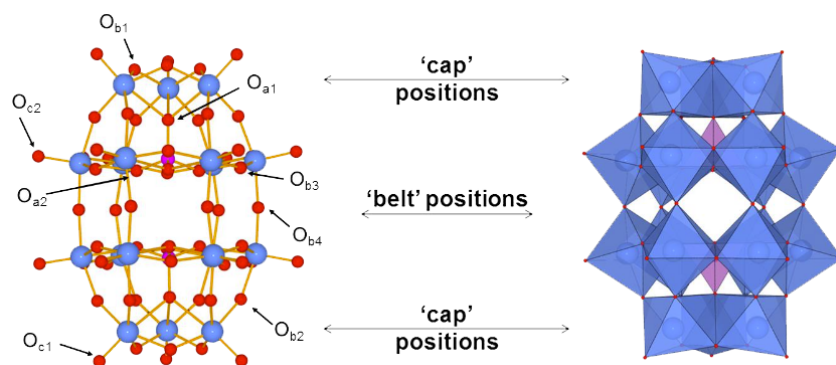


Figure 1.9: The Wells-Dawson polyoxometalate represented by ball and stick (left) and polyhedral (right) structures.

Rotational isomerism can be obtained by successive 60° rotation around the three-fold axis of the end caps M_3O_{13} culminating in three isomers, parent α -Dawson (D_{3h} symmetry), β isomer (C_{3v} symmetry), γ isomer (D_{3d} symmetry). Furthermore, with the rotation of the entire $[XM_9O_{34}]^{n-}$ half unit, three possible isomers α^* (D_{3d} symmetry), β^* (C_{3v} symmetry), γ^* (D_{3d} symmetry) can be derived from α , β and γ structures (Figure 1.10). There is clear stability trend for these isomers : $\alpha > \beta > \gamma > \gamma^* > \beta^* > \alpha$ ^[27,28], but only α ^[29], β ^[30], γ ^[31,32] and γ^* ^[33] structures have been isolated.

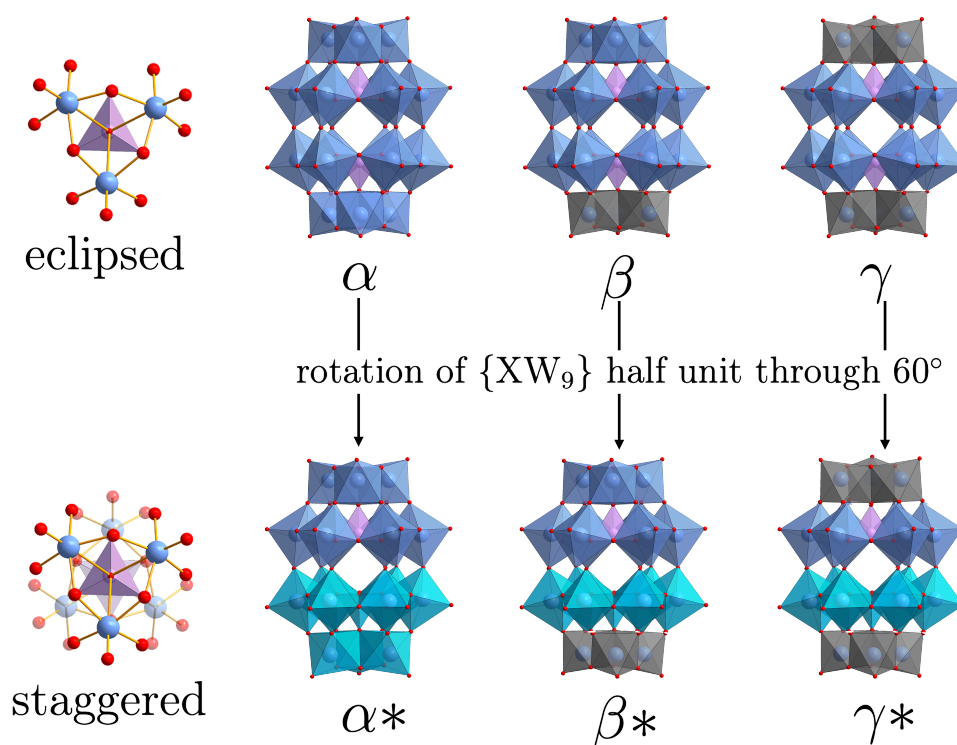


Figure 1.10: The six possible isomers of the Wells-Dawson polyoxometalate^[34]

In some POM structures, mainly Keggin and Dawson type anions, one or more of the addenda atoms can be removed by controlling the pH. As mentioned in 1.1.1, the incomplete structure is defined as lacunary POM. Lacunary POMs can be easily generated and stable^[35], which contributes largely to POM chemistry. With the removal of addenda centres, the overall charge and charge density increase and anionic bridging oxo ligands are exposed as polydentate inorganic ligands capable of binding new cationic species, leading to higher reactivity of the cluster. It's considered that among all kinds of POMs, the structures of Polyoxotungstates (POTs) are the most kinetically inert^[36], which results in the richest lacunary chemistry and the only addenda species to form stable enough lacunary species to isolate. Correspondingly lacunary-polyoxomolybdates have high reactivity and hard to isolate. For the Wells-Dawson POM, a family of lacunary variants can be generated by treating the plenary cluster with base. By removing a single metal, a cap or a face, three lacunary species are formed, respectively the mono-lacunary $[X_2M_{17}O_{61}]^{(n+4)-}$ ^[37], the tri-lacunary $[X_2M_{15}O_{56}]^{(n+6)-}$ ^[38] and the hexa-lacunary $[X_2M_{12}O_{48}]^{(n+8)-}$ ^[39] (Figure 1.11). Only the α -Dawson structure can give stable and isolable lacunary clusters, and only the mono-lacunary $[X_2M_{17}O_{61}]^{(n+4)-}$ species shows positional isomerism, distinguished by having the addenda metal removed from a cap or belt position.

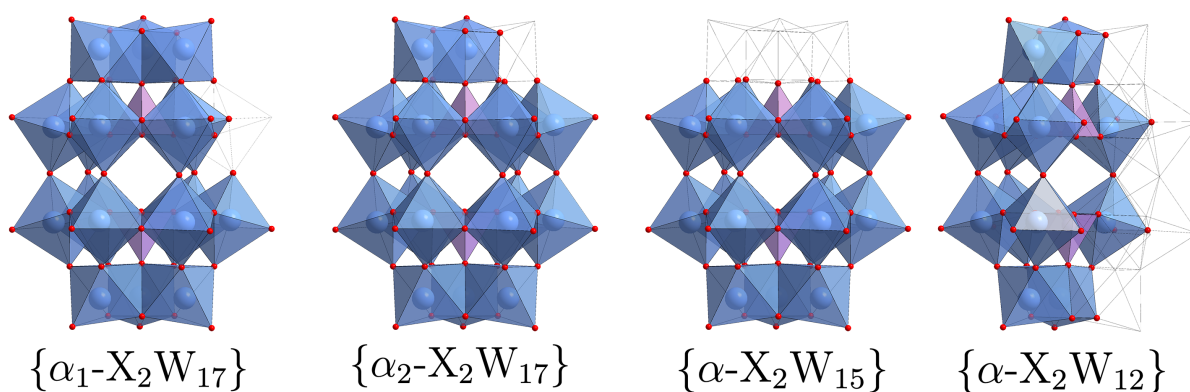


Figure 1.11: The four possible lacunary Dawson clusters, in which α_1 -species are those with an addendum removed from cap positions and α_2 -species are those with an addendum removed from the belt positions.

1.2 Electronic and Photocatalytic Properties of POMs

One of the most attractive features of POMs is their complex electronic character and as such POMs are mostly applied in photo-, electro- and thermal catalysis fields^[40]. Although POMs can vary widely in terms of composition, size and structure, the electronic properties of the metal-oxo building blocks largely govern the electronic properties of POMs. Normally POMs are composed of early transition metal cations in their highest oxidation states, thus the central metals can be reduced making POMs act as electron reservoirs^[41]. The highest occupied molecular orbitals (HOMO) in POMs are mostly 2p of the bridging oxygens, and the lowest unoccupied molecular orbital (LUMO) are a mixture of 2p and 4d of the molybdenum atoms with anti-bonding π character^[42], and the redox properties of the substituted cluster depend largely on the LUMO energy. According to molecular orbital theory, class I and class III structures have vacant non-bonding t_{2g} orbitals to be populated on reduction as a result of having one terminal oxo bond in octahedral unit. For class II POMs, whose t_{2g} orbitals are involved in π -bonding^[43], this is not possible. That means in structures with lower HOMO-LUMO (H-L) gap, including Lindqvist, Keggin and Dawson anions can undergo reversible reductions of metal centres

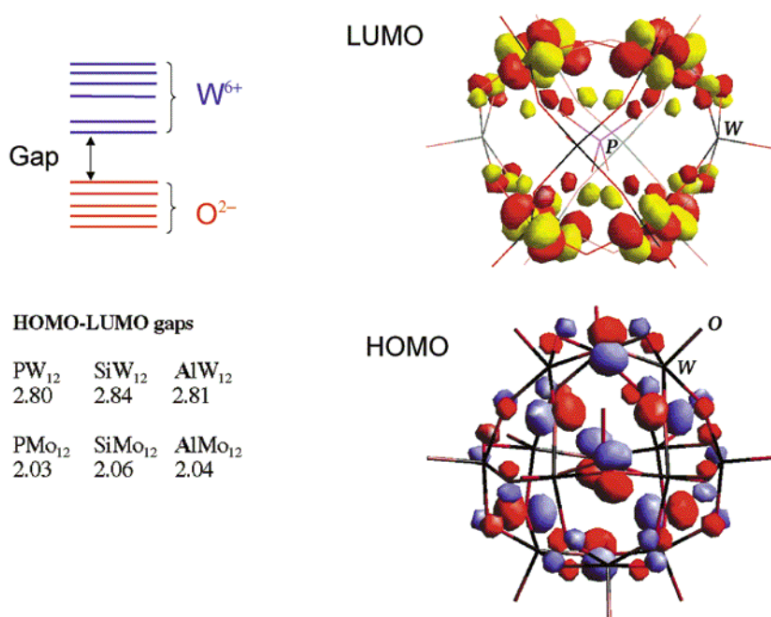


Figure 1.12: Molecular orbitals scheme for a α -Keggin anion, where H-L gap is represented by the separation between M and O²⁻ bands. Figure reproduced from reference 44.

(Figure 1.12). The non-bonding nature of orbital in class I and class III POMs results in good acceptance of electrons onto the structures, for which electrons can be loaded and unloaded reversibly. The number of electrons accepted by a fully oxidised POM structure can be determined by a rule which is applicable to all redox rich POMs^[45]. For POMs with same addenda atoms, it is related to q/m , where q is the overall charge of the clusters and m is the number of metal ions. The larger and lower the negative charge of the POM is, the easier for it to be reduced. For POMs with different addenda metal atoms but with the same structure, the LUMO energy increases as the electronegativity of the d^0 metal ion decreases (Figure 1.13)^[27].

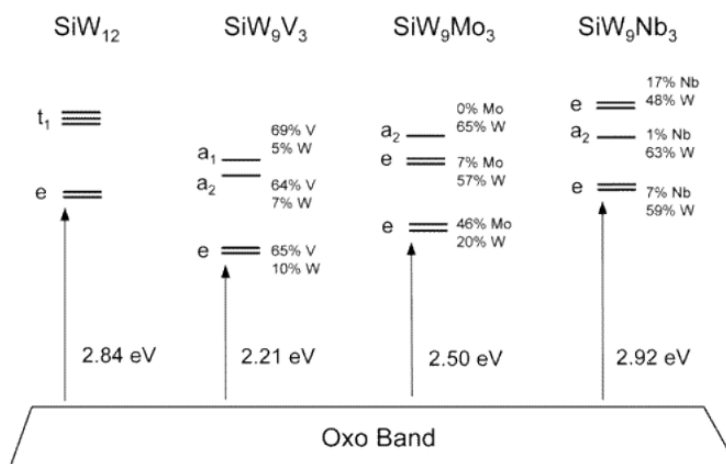


Figure 1.13: effect of the electronegativity of the metal atom on the HOMO-LUMO gap of POMs. Figure reproduced from reference 27.

Another factor affecting the LUMO energy which only happens in heteropolyoxometalates is the size of templating anion. For heteroatoms of the same charge, smaller atom can cause more negative potential which makes it harder for POM to accept electrons^[27]. When the POM structures are reduced, inter-valence charge transfer (IVCT) is observed which means electrons transfer rapidly between metal centres under thermal assistance (Figure 1.14), which creates strong absorptions in the infrared and low energy visible spectrum, giving a strong blue coloration. For POMs like Keggin and Lindqvist types, the structures are highly symmetrical and each metal site is equivalent, which results in "hopping" within the entire clusters. For structures with different metal centres like the Dawson type, delocalisation happens between equivalent metal centres. These bands

effectively reflect the progress of reduction, and further addition of electrons can lead to new IVCT bands at specific wavelengths. Therefore, IVCT bands are powerful to monitor the reduction states of POMs in solution.

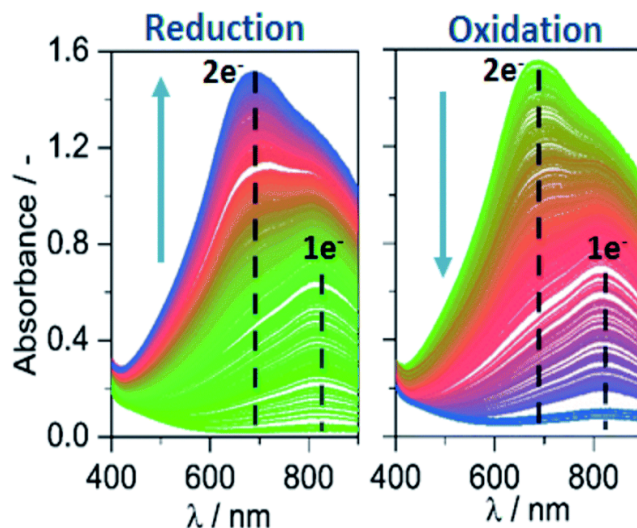


Figure 1.14: UV-vis spectra showing the reversible growth of the IVCT band upon reduction and reoxidation of the POM. Figure reproduced from reference 46.

The interaction between POMs and light is an efficient way to access their rich electronic properties. For class I and class III POMs, which can access the ligand to metal charge transfer (LMCT) bands of their terminal metal-oxygen bonds, they are inherently photoactive compounds. During the photo-excitation of the $O \rightarrow M$ band, an electron is promoted from the doubly occupied 2p orbital of the oxygen (HOMO) to the empty d orbitals of the metal (LUMO) (Figure 1.15), so the charge transfer represents the HOMO-LUMO gap of the compound.

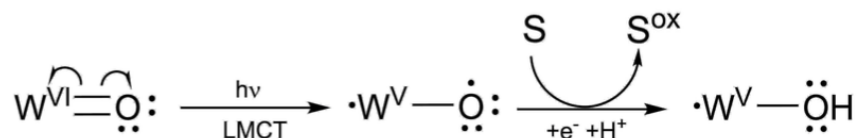


Figure 1.15: Mechanism of photoexcitation of the LMCT band and substrate oxidation. Figure reproduced from reference 20.

These LMCT bands are normally located in the UV region of the spectrum, but some tailing can occur in the visible region by employing more electronegative metal ions to

lower the LUMO energy of POM. Upon excitation of the LMCT band, a d1 electron is generated on the metal centre and a radical cation entered on oxygen exists in a triplet state with a short lifetime. Then, depending on the substrate, this state is quenched to an oxygen radical by hydrogen atom transfer (HAT) or single electron transfer (SET). A new O–H bond is formed and the d1 electron is trapped on the metal as a result of this oxygen radical affording the POM reduction and substrate oxidation. Then blue coloration can be present upon irradiation resulted by IVCT as previously described. The IVCT band however is photochemically inactive as it does not generate radical cations. As POMs can accept electrons and protons from substrates under irradiation reversibly, it is attractive to oxidise substrates with POMs as catalysts.

POMs can preassociate with substrates directly via hydrogen bonding or mediated by water molecules, which has been proved by ultrafast electron transfer dynamics. Subsequently, either HAT or SET mechanisms lead to POM reduction and substrate oxidation, and then dissociation of the reduced POM and oxidised substrate. Then depending on the availability of protons in the system, dioxygen is reduced to either superoxide, hydroperoxide or water, a sacrificial electron acceptor is reduced and the POM is re-oxidised to close the cycle (Figure 1.16)^[47].

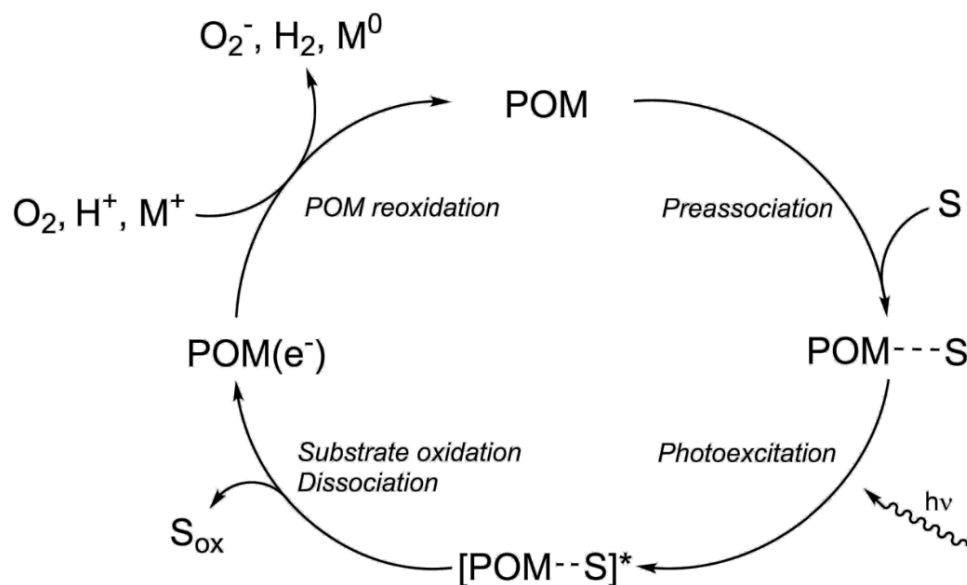


Figure 1.16: Catalytic cycle of POMs upon photocatalytic reactions, adapted from reference 47.

As discussed above, the solvent environment can decide the mechanism of substrate oxidation. In aqueous systems, hydroxyl radicals are generated by photo-irradiation on the pre-association complex between the POM and water. Usually organic compounds are then totally mineralised as the hydroxyl radicals are powerful oxidants, and the indirect oxidation of substrates photo-catalysed by POMs in aqueous solution is now applied in the degradation of organic pollutants^[48]. In non-aqueous solvents, the substrates are able to be oxidised under control as pre-association complex is formed directly between POM and substrate, therefore organic molecules can be selectively oxidised by POM photocatalysis in non-aqueous systems^[49].

1.3 Hybridisation of POMs and Photocatalytic Applications

As described in 1.1.1, polyoxometalates are widely applied from nano- to meso-scale as a result of their ability to form nearly infinite variety of structures from simple metal oxide units^[2]. However, this field can be extended to an even greater amount by reacting POM clusters with other organic species so that the properties of POM can be modified and new specific functions can be added. Hybrid-POMs is a wide-ranging concept covering new species formed from POMs combined with various organic components.

Perhaps the most attractive and fast-growing area in POM chemistry field is the inorganic-organic hybrid polyoxometalates, which involves the association of organic components with POMs, referred to as hybrid-POMs^[50]. These class of materials can be further divided into two distinct subtypes by interaction types between the two components^[51]. In class I, the organic moiety is associated with POM through electrostatic interactions, hydrogen bonding or Van der Waals interactions. They can be formed easily by ion exchange reactions between the two precursor salts dissolved in solution. However, further salt exchange reactions may result due to the weak interactions between the two components, often leading to the loss of components, making the application of these hybrids limited.

In class II systems, the organic moieties are directly grafted to the POM by covalent bonds or coordination bonds. An anchorage point on the POM is needed to reinforce the linking between POM and organic component, this can be the metal centre for nitrogen atoms (through metal-nitrogen bonds) or more commonly seen in POM functionalisation, the periphery oxygen atoms for p-block elements (through M-O-X bonds, X= S, P, As, Sn, Ge...)^[1]. Figure 1.17 shows some typical class II covalent hybrid connectors.

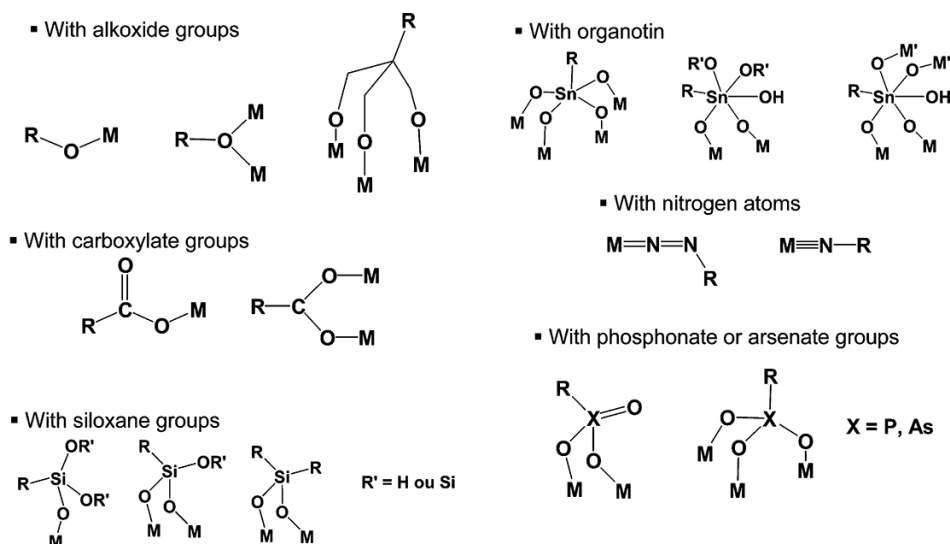


Figure 1.17: Class II covalent hybrid connectors, reproduced from 1.

The methods of synthesis are highly specific in accordance with both the POM structure and addenda atoms, such as imido-functionalisation for Lindqvist hexamolybdate through

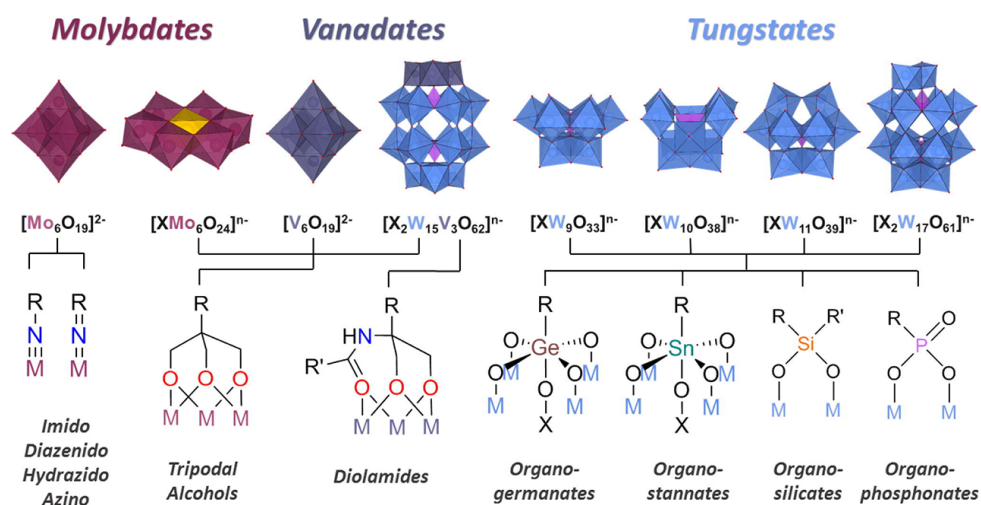


Figure 1.18: Covalent organofunctionalisation routes for archetypal POM structures, reproduced from reference 52.

to nucleophilic addition-substitution reactions and tripodal alcohols for Anderson-type molybdates (Figure 1.18)^[52]. For Keggin and Dawson type polyoxotungstate anions, covalent hybridisation can be accessed via lacunary species. Upon removing one or more tungsten atoms, oxygen atoms with negative charge are exposed at the vacant position for further reactions with various oxyphilic organic reactants, for example in mono-vacant species four oxygen atoms present as a square geometry and in tri-vacant heteroPOMs six oxygen atoms present as a hexagon acting as binding sites exposed at the surface of the POMs (Figure 1.19).

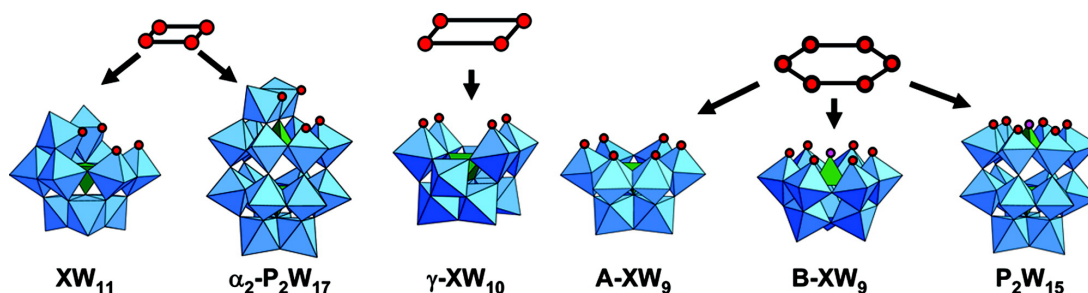


Figure 1.19: Oxygen atoms binding sites for lacunary Keggin and Dawson POMs, reproduced from 1.

The richness of organic moieties allows endless possibilities for new organofunctionalised POMs^[53,54]. Figure 1.20 shows some specific examples of hybrid-POMs with phosphonic acid, silicic acid and organotin cross-linking sites. The cross-linking mode between the organic moiety and the POM decides the coordination angle and the redox behaviour of the hybrid-POM. Specifically, the phosphonate hybrid POM is of particular interest for the structural feature that there are two protruding oxygen atoms at the bridge between the POM and the organic ligand, which could be an active site with various metal ions introduced for catalytic reactions and tuning the redox properties of POM^[20]. Moreover, upon hybridisation with an organic ligand containing a phosphonic acid group, the cross-linking site of hybrid-POM can achieve an angle close to 180°. Therefore, higher-order structures can be expected with design of phosphonic acid-containing organic ligands.

POMs have been deeply studied as oxidation photocatalysts and electrocatalysts in acid^[55]. Class I hybridisation in particular allows ready functionalisation of the POM with photosensitisers using simple synthesis routes. They can be formed by combination between

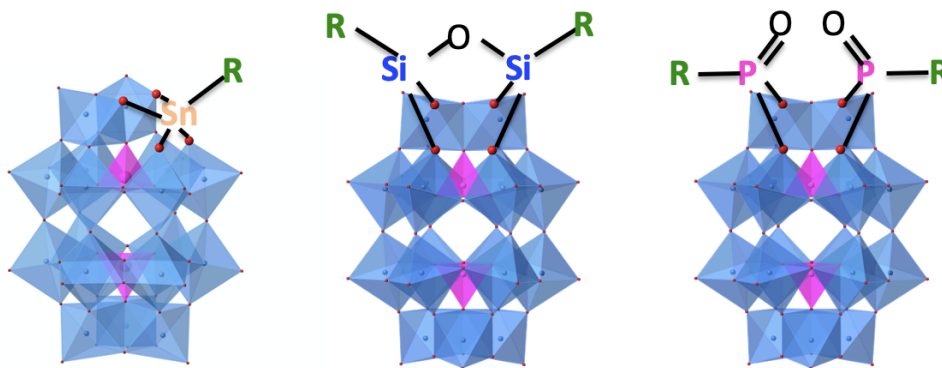


Figure 1.20: Examples of hybrid POMs formed from mono-lacunary Dawson POMs and various organic ligands (R)

photosensitive cations and POM anions at a justified ratio based on charge balancing, and the absorption spectrum are normally wide as a result of overlay of the absorption profiles of two components. As POMs strong electron acceptors, charge transfer salts with new absorption bands can form when POMs are paired to electrons donator organic cations, In 2019, Bonchio et al. reported a novel class I hybrid POM water-oxidation catalyst formed by interaction between a Ru_4POM and perylene-bisimide (PBI) cations (Figure 1.21) [56]. $[\text{Ru}_4\text{POM}]^{10-}$ is combined in stoichiometric quantities with 5 eq $[\text{PBI}]^{2+}$ and caged by the cations forming a core-shell nano-cylinder by self-assembling. It has broad redshifted light-harvesting ability and shows favourable exciton accumulation, and can be photoexcited by visible light to achieve efficient oxygen evolution.

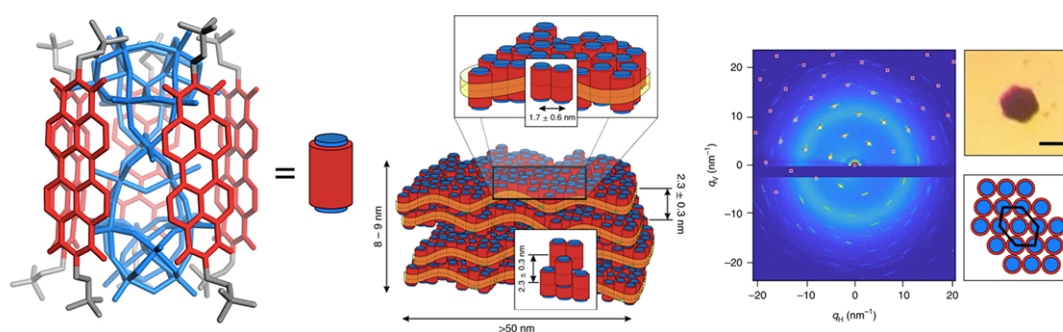


Figure 1.21: Photosynthetic assembly and cylindrical aggregates of the PBI- Ru_4POM reported by Bonchio et al., reproduced from reference 56.

Although it is quite convenient to widen the absorption range of POMs by class I hybridisation, the control of the spatial relationship is limited and it is hard to predict

charge transfer between the two components. Therefore with the tuneable reactivity and the potential for electronic coupling, class II hybrid POMs have a broader way for proposed applications in photochemistry. In hybrid-POM systems, the spatial configuration is extremely essential for the photo induced charge separation lifetime^[57], which can be controlled to a rare degree by covalent coupling of the organic moiety to specific sites on the POM. The most frequently studied photoactive class II hybrid POMs are usually chromophores which are covalently attached to Keggin and Dawson polyoxotungstates for their useful redox properties. In 2013, Proust et al. reported a class II hybrid POM using an iridium photosensitiser covalently grafted to a Dawson-type polyoxotungstate (Figure 1.22)^[58]. The hybrid displays some desirable properties including performing photocatalytic hydrogen production stably under visible light in the presence of triethylamine as a sacrificial electron donor and forms a one-electron reduced species at a fast rate. Although the turnover frequency is not so promising, it shows the potential for Dawson POMs acting as the basis of modular and functional class II hybrid POM photoelectrocatalysts.

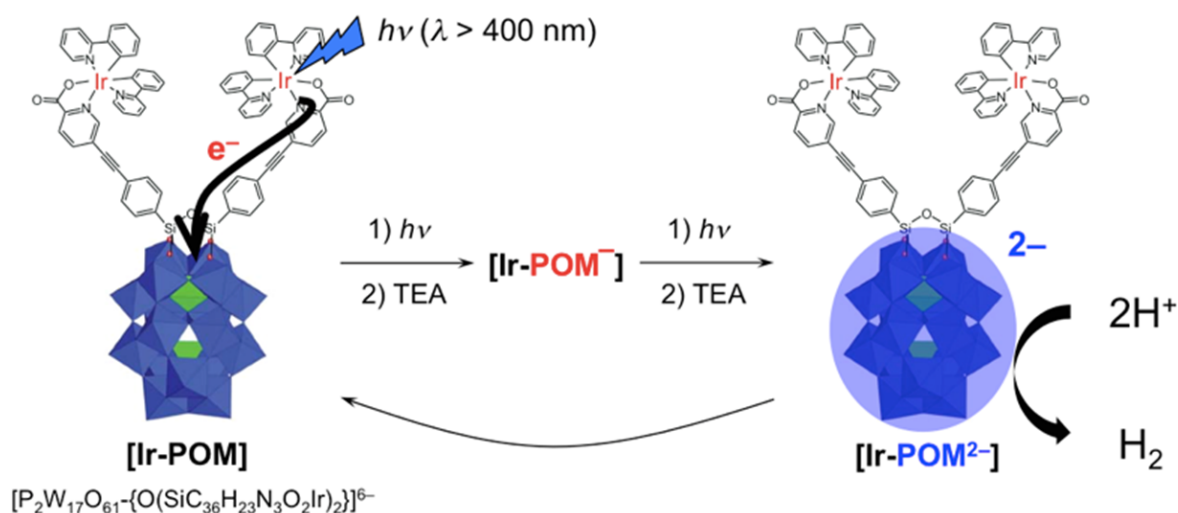


Figure 1.22: Reversible hydrogen production under visible light in the Ir(III)-POM reported by Proust et al., adapted from reference 58.

2 Aims

The aim of this report is to explore POM hybridisation for photochemical applications. We will explore adding an organic ligand to act as a light-harvesting component with the ability to transfer electrons to POMs, so that new photocatalytic dyad-type systems can be developed. Moreover, if long-lived charge separated states can be achieved, then the system should be able to act as an effective photocatalyst under visible light irradiation. We chose perylene diimide dyes (PDI dyes) for their thermal and redox stability, high absorption of visible light and relatively low cost. The target materials were class II hybrids formed from the lacunary Wells-Dawson polyoxotungstate anion modified with a new bis-phosphonate PDI dye, N,N'-bis(phosphonomethyl)-3,4,9,10-perylenediimide (**PMPDI**). In particular, the symmetry and bis-functionality of **PMPDI** is expected to allow both monomeric and polymeric species to be isolated.

The target hybrid materials will be synthesised and characterised using a range of analytical techniques. Electrochemical- and photo-chemical characterisation will also be employed to assess the extent of the redox tuning and photocatalytic performance of the new compounds, and will be compared to the precursor components.

3 Results and Discussion

3.1 Synthesis and Characterization of Polyoxometalate Starting Materials

Polyoxotungstates commonly form Keggin and Dawson structures which are thermodynamically stable and can more easily form hybrid POMs with organic ligands. As POMs can act as reservoirs for both protons and electrons, they have shown great potential in catalysis^[59]. To achieve our goal of a POM based catalytic platform, the first step is to synthesis a lacunary species of Wells-Dawson polyoxotungstate $K_{10}[P_2W_{17}O_{61}]$ (**P₂W₁₇**).

A self-assembly reaction in aqueous media is carried out to form the Dawson polyoxotungstate $K_6[P_2W_{18}O_{62}]$ (**P₂W₁₈**).^[60] The tetrahedral $[WO_4]_2^-$ fragments from $Na_2WO_4 \cdot 2H_2O$ is expanded on acidification to protonated metal-hydroxide complexes $[WO_2(OH)_4]_2^-$,^[61] which tends to form octahedral coordination through oligomerisation and condensation reactions as the precursors to condense to reactive metal-oxide fragments. The PO_4^{3-} from H_3PO_4 acts as template for the polyoxometalate to self-assemble upon further addition of acid^[62]. K^+ from KCl provides cations to precipitate the resultant product^[63]. A mono-lacunary Wells-Dawson structure with a free binding site is needed for the organic ligands incorporation. As POMs are unstable in alkaline conditions, we were able to exploit this characteristic to remove one W=O group in the **P₂W₁₈** by exposing it to base, resulting in the α -configuration mono-lacunary Dawson cluster with a binding sites for our organic moieties.^[37]

^{31}P NMR confirmed the formation and structures of P_2W_{18} and P_2W_{17} . The two template phosphate oxalate-anions in $[\text{P}_2\text{W}_{18}\text{O}_{62}]^{6-}$ have the same environment and therefore the same chemical shift (Figure 3.1 left), while there are two environments for $[\text{PO}_4]^{3-}$ in $[\text{P}_2\text{W}_{17}\text{O}_{61}]^{10-}$. The phosphorus at the closed end of POM clusters is more shielded matching the chemical shift $\delta = -14.36$ ppm whilst the one closer to the open binding site is de-shielded and is represented by $\delta = -7.22$ ppm. The data shown in Figure 3.1 (right) represents a pure product of mono-lacunary Dawson structure POM P_2W_{17} .

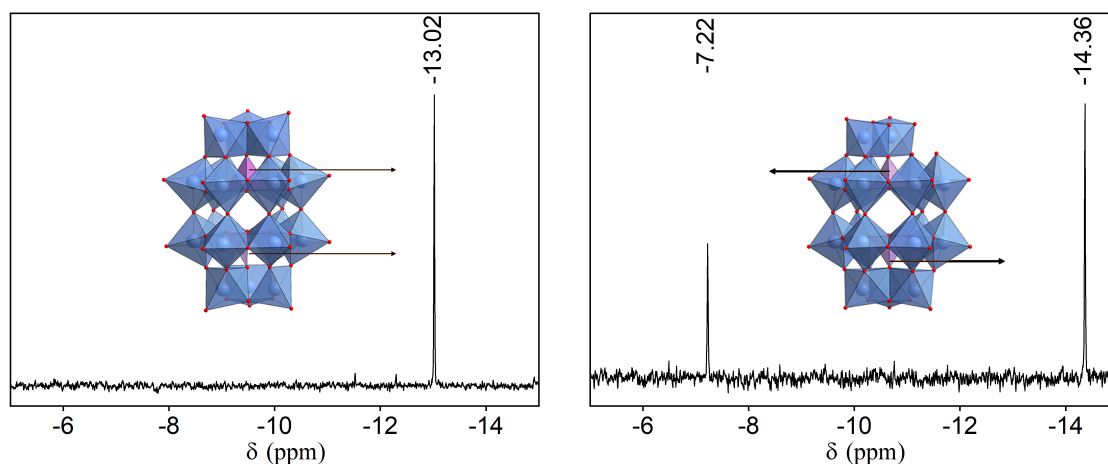


Figure 3.1: ^{31}P NMR spectrum displays a single peak for the template $[\text{PO}_4]^{3-}$ in $[\text{P}_2\text{W}_{18}\text{O}_{62}]^{6-}$ at $\delta/\text{ppm} = -13.02$ (left) and the $[\text{P}_2\text{W}_{17}\text{O}_{61}]^{10-}$ displays two peaks at $\delta/\text{ppm} = -7.22$ and -14.36 (right).

ESI-MS was employed as a supplementary technique to confirm the identity of the POMs. The results showing POM anions fragments confirmed the successful synthesis of P_2W_{18} and P_2W_{17} (Figure 3.2, Table 3.1 and 3.2).

Table 3.1: Selected mass spectrometry peak assignments for P_2W_{18}

Assignment	z	m/z (calc)	m/z (obs)
$\{\text{K}_2\text{H}[\text{P}_2\text{W}_{18}\text{O}_{62}]\}$	3-	1480.56	1480.40
$\{\text{K}_2\text{Na}[\text{P}_2\text{W}_{18}\text{O}_{62}]\}$	3-	1487.88	1487.71
$\{\text{K}_2\text{NaH}[\text{P}_2\text{W}_{18}\text{O}_{62}]\}$	2-	2232.3	2232.3
$\{\text{K}_3\text{H}[\text{P}_2\text{W}_{18}\text{O}_{62}]\}$	2-	2240.3	2240.2
$\{\text{K}_3\text{Na}[\text{P}_2\text{W}_{18}\text{O}_{62}]\}$	2-	2251.31	2251.15

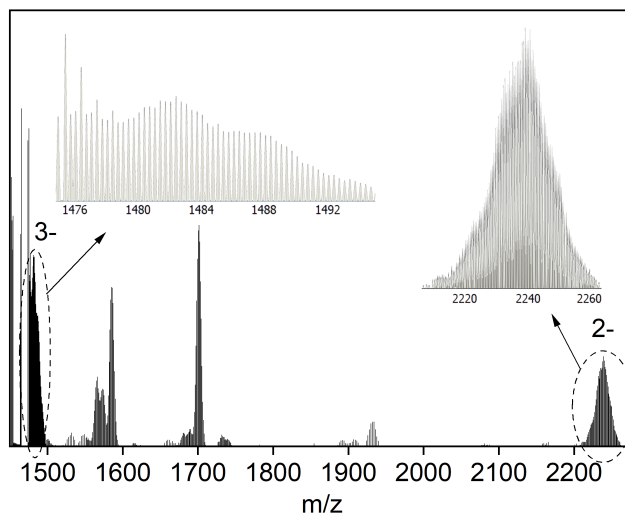


Figure 3.2: Negative mode ESI-MS spectrum of $\mathbf{P}_2\mathbf{W}_{18}$ in the m/z range 1450 - 2300

Table 3.2: Selected mass spectrometry peak assignments for $\mathbf{P}_2\mathbf{W}_{17}$

Assignment	z	m/z (calc)	m/z (obs)
$\{\text{H}_8[\text{P}_2\text{W}_{17}\text{O}_{61}]\}$	2-	2085.43	2085.4
$\{\text{K}_2\text{H}_6[\text{P}_2\text{W}_{17}\text{O}_{61}]\}$	2-	2123.39	2123.36
$\{\text{K}_5\text{Na}_2\text{H}[\text{P}_2\text{W}_{17}\text{O}_{61}]\}$	2-	2202.85	2202.74

3.2 Synthesis and Characterization of PMPDI

On building a suitable organic-inorganic hybrid POM photocatalytic system, it is crucial to find an organic ligand with strong visible-light absorption that is able to form stable hybrid with $\mathbf{P}_2\mathbf{W}_{17}$. As a result, we looked into perylene diimide dyes (PDI dyes), for they not only have robust properties but also are low cost industrial dyes used as colorants^[64]. PDIs are thermally stable with decomposition temperatures normally over 300 °C^[65]. In addition, they are highly oxidatively stable both in air and a range of solvents^[66], making it possible to hybridise them with the POM. As the highly nucleophilic oxygen atoms in lacunary Dawson polyoxotungstate can react with organophosphorus reagents, it is an effective method to modify the electrochemical properties and photochemical reactivity of POMs to graft organophosphonate groups to the POM core. With a relatively low pKa at 1.86^[67], the $-\text{PO}_3\text{H}_2$ group has a high proton dissociation. Therefore, we chose a PDI

derivative N,N'-bis(phosphonomethyl)-3,4,9,10-perylenediimide (**PMPDI**, Figure 3.3) as the organic ligand. **PMPDI** is anionic so there is no cation interaction with POM, and the phosphonate groups contribute to synthesising stable hybrid materials^[68]. **PMPDI** is therefore a suitable component for our building block strategy for new material design.

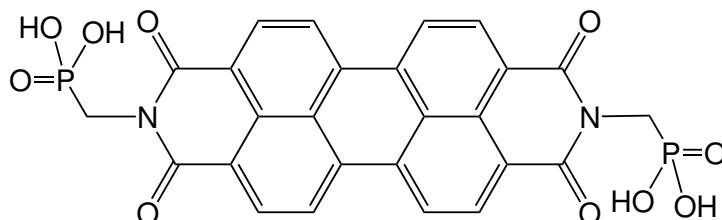


Figure 3.3: Structure of N,N'-bis(phosphonomethyl)-3,4,9,10-perylenediimide (**PMPDI**)

PMPDI is synthesized by a dehydration reaction between perylenetetracarboxylic dianhydride (PTCDA) and (aminomethyl)-phosphonic acid in molten imidazole^[67]. In this nucleophilic substitution reaction, the amino as nucleophilic source attacks the anhydride, the lone pair on amino N flows to carbonyl C of the acid anhydride to form an amide bond, and the acid anhydride is hydrolysed to a carboxyl group and an amide. Then the lone pair on imino N attacks the carboxyl group C to form another amide bond with dehydration (Figure 3.4).

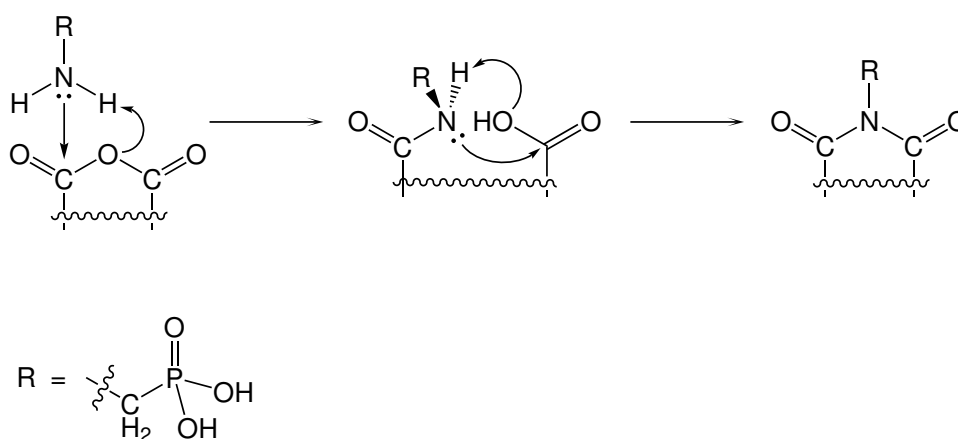


Figure 3.4: Mechanistic detail of the anhydride hydrolysis reaction

Purification of the product can be achieved by adjusting the pH. By suspending the crude product in water and adding base, **PMPDI** can be deprotonated and form tetra-

potassium salt to dissolve, whilst the starting material PTCDA is not soluble until pH 9.5 and can be filtered to remove. Then by adding HCl to make **PMPDI** precipitate in acidic solution, it can be separated from imidazole. The product was characterised by proton and phosphorus NMR. KOH was employed to increase the solubility of **PMPDI** resulting in a peak for hydroxide in proton NMR. By increasing pH, the deprotonated **PMPDI** gives a color change from deep red to light yellow in aqueous solution. Due to the poor solubility, the phosphorus NMR was run for an extended time (13.36 h) to achieve a higher signal to noise ratio. The proton NMR shows highly broadened peaks for aromatic protons at around 7.85, which happens commonly for PDIs due to π -stacking aggregation^[69,70], and a sharp peak at around 4.16 for the methylene protons (Figure 3.5 left). The ratio is 2 : 1 which matches the expected for **PMPDI**. There is only one peak at 12.18 for the phosphorus NMR (Figure 3.5 right) showing no (aminomethyl)-phosphonic acid or any side product containing phosphorus in the sample.

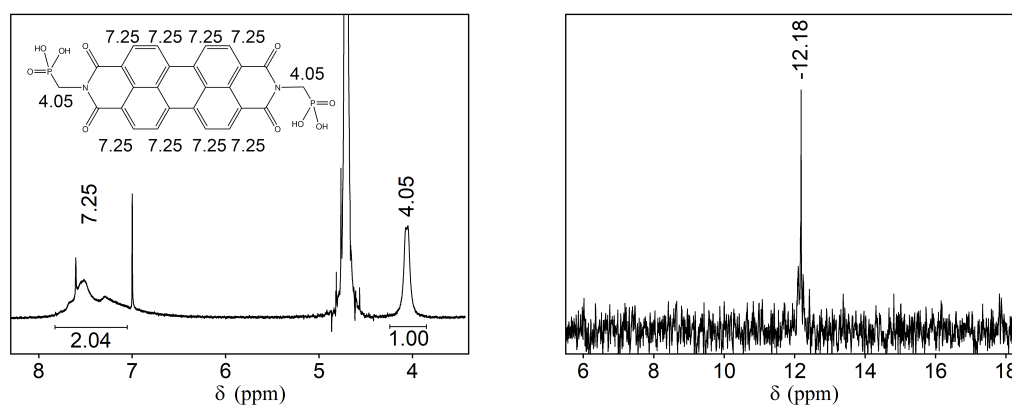
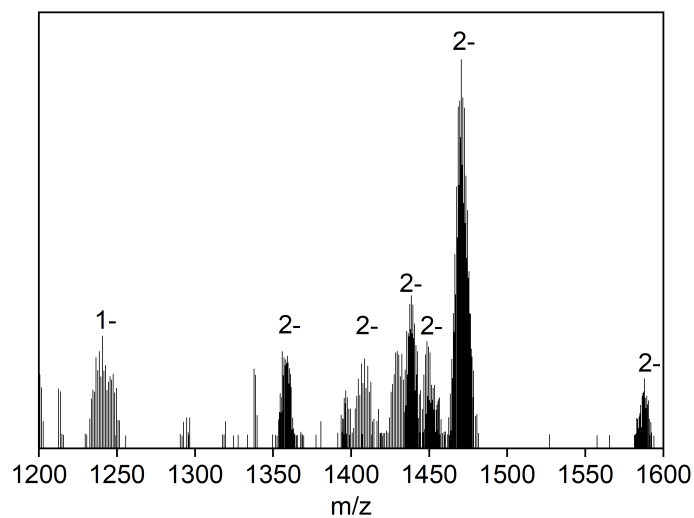


Figure 3.5: ¹H NMR (left) and ³¹P NMR (right) spectrum for **PMPDI**

Mass spectrometry was employed to characterise the product. However we were not able to find an appropriate solvent to perform MS, the only solvent that can dissolve **PMPDI** is alkaline aqueous solution, but base should not be applied to interfere the spectrum. The result showed that the **PMPDI** molecules stacked to each other and formed some dimer, tetramer and pentamers anions (Figure 3.6 and Table 3.3).

Table 3.3: Selected mass spectrometry peak assignments for **PMPDI**

Assignment	z	m/z (calc)	m/z (obs)
$\{\text{Na}_4\text{H}_3[\text{C}_{26}\text{H}_{12}\text{O}_{10}\text{N}_2\text{P}_2]_2\}$	1-	1242.97	11242.63
$\{\text{Na}_6\text{K}_7\text{H}[\text{C}_{26}\text{H}_{12}\text{O}_{10}\text{N}_2\text{P}_2]_4\}$	2-	1354.84	1354.58
$\{\text{Na}_2\text{H}_{16}[\text{C}_{26}\text{H}_{12}\text{O}_{10}\text{N}_2\text{P}_2]_5\}$	2-	1466.54	1466.54
$\{\text{Na}_4\text{K}_{14}[\text{C}_{26}\text{H}_{12}\text{O}_{10}\text{N}_2\text{P}_2]_5\}$	2-	1467.72	1467.53
$\{\text{Na}_3\text{K}_{15}[\text{C}_{26}\text{H}_{12}\text{O}_{10}\text{N}_2\text{P}_2]_5\}$	2-	1475.71	1475.52
$\{\text{Na}_6\text{K}_4\text{H}_8[\text{C}_{26}\text{H}_{12}\text{O}_{10}\text{N}_2\text{P}_2]_5\}$	2-	1586.42	1586.46
$\{\text{Na}_8\text{K}_9\text{H}_1[\text{C}_{26}\text{H}_{12}\text{O}_{10}\text{N}_2\text{P}_2]_5\}$	2-	1703.85	1703.85

Figure 3.6: Negative mode ESI-MS spectrum of **PMPDI** in the m/z range 1200 - 1600

According to the literature^[67], some PTCDA can form by slow hydrolysis of **PMPDI**, so we performed CHN elemental analysis to confirm the purity, and the result (Table 3.4) was consistent with the relatively pure hydrate mono-potassium salt of the product ($\text{K}[\text{PMPDI-H}] \cdot \text{H}_2\text{O}$).

Table 3.4: Result obtained for CHN elemental analysis of **PMPDI** compared to the predicted values

	%C	%H	%N
Predicted	49.22	2.70	4.42
Observed	49.1	2.9	5.1
	49.28	2.82	5.01

3.3 Synthesis of the PMPDI-POM Hybrid (I and II)

The hybrid POM complex compound **I**, $[\text{C}_2\text{H}_6\text{N}]_6\text{H}_4[\text{P}_2\text{W}_{17}\text{O}_{61}((\text{P}=\text{O})\text{C}_{26}\text{H}_{12}\text{O}_7\text{N}_2\text{P})_2] \cdot 14\text{H}_2\text{O}$ (Figure 3.3) was synthesised in good yield by modifying a literature procedure for a similar 4-carboxyphenyl phosphonic acid functionalised cluster^[71]. The condensation of **PMPDI** with the lacunary precursor **P₂W₁₇** in acidified dimethylacetamide (DMA) and water yielded a red powder. A high temperature and a long reaction time might cause impurities as a result of the formation of **P₂W₁₈**, but contribute to the dissolution of reactants and the occurrence of reactions. We tried a series of temperatures and times and found that the best condition is 130 °C and 18 hours with 10 eq HCl added. PTCDA has poor solubility in acetonitrile and DMA especially in acidic environments, so water was added to act as solvent (50% by volume).

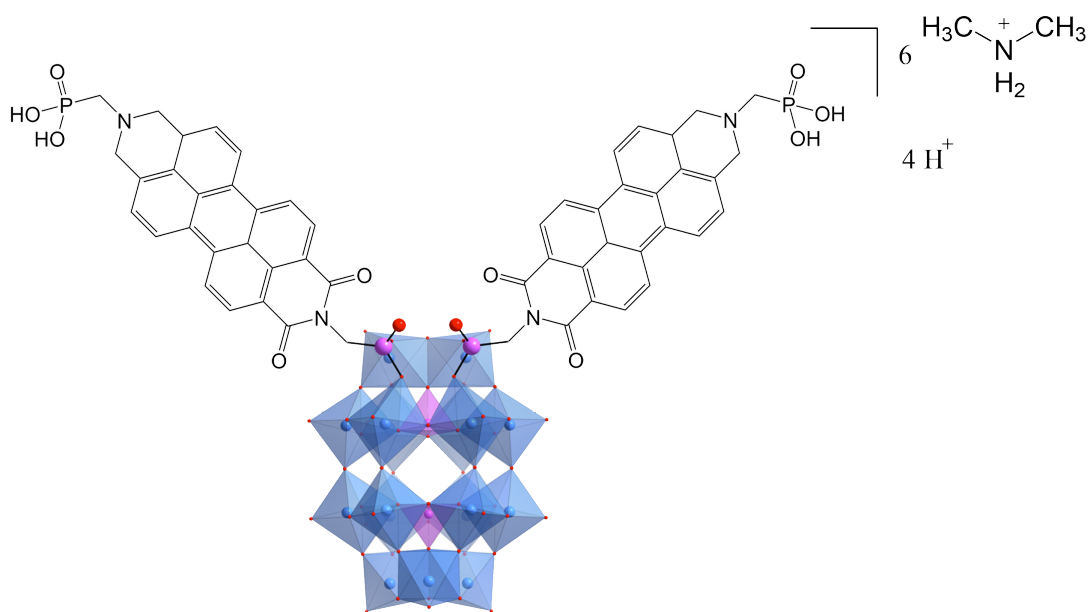
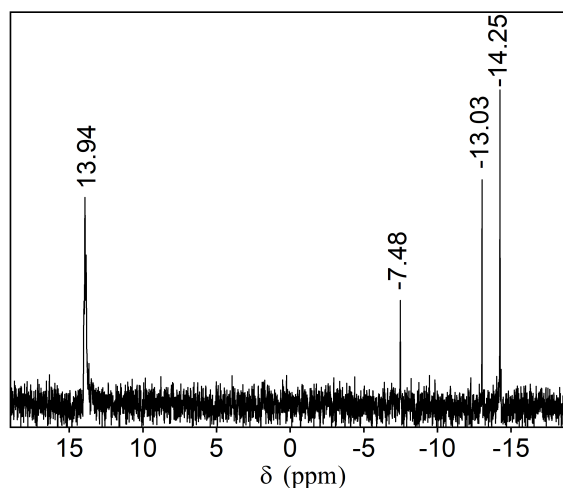
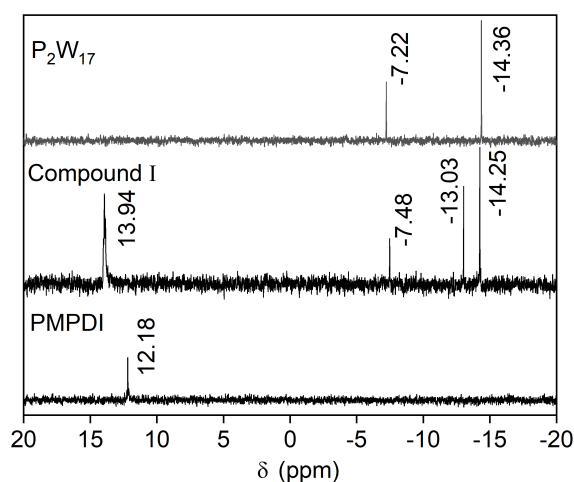


Figure 3.7: Structure of Compound **I**

Compound **I** was structurally characterised by ³¹P NMR, which presented four peaks at $\delta/\text{ppm} = 13.94, -7.49, -13.03$ and -14.25 (Figure 3.8). The solubility of the hybrid in water is quite good but as a result of π -stacking aggregation caused by the aromatic organic ligand, the signal is not so obvious even using a longer term NMR experiment (1.48 h).

Figure 3.8: ^{31}P NMR spectrum for compound I

As shown in previous work in our group^[71], the phosphorus in the closed end of the POM should be slightly de-shielded compared to that of P_2W_{17} matching the shift for the peak from $\delta/\text{ppm} = -14.36$ to $\delta/\text{ppm} = -14.25$. For the phosphorus adjacent to the lacunary position, it will be more shielded, matching the shift from $\delta/\text{ppm} = -7.22$ to -13.03 . The two phosphorus in the **PMPDI** are initially in the same environment but after the hybridisation, the one occupying the lacunary site at the vacant cap position of P_2W_{17} should be shielded, whose peak is shifted from $\delta/\text{ppm} = 12.17$ to $\delta/\text{ppm} = -7.5$, whilst the one at the terminal end of **PMPDI** undergoes a minor downfield shift from $\delta/\text{ppm} = 12.17$ to $\delta/\text{ppm} = 14$ (Figure 3.9).

Figure 3.9: ^{31}P NMR spectrum stacked for P_2W_{17} , compound I and **PMPDI**

Mass spectrometry was performed to characterise the compound **I** (Figure 3.10 and Table 3.5), however, as compound **I** has poor solubility in acetonitrile and methanol, the signals were too weak to distinguish, therefore we used water as solvent. Under electron ionisation in gas phase, the molecular ion undergoes fragmentation, and we only detected some fragments of P_2W_{17} anions and **PMPDI** anions. Compound **I** is therefore unstable under high temperatures or strong electric fields encountered in the mass spectrometer.

Table 3.5: Selected mass spectrometry peak assignments for compound **I**

Assignment	z	m/z (calc)	m/z (obs)
$\{\text{K}_2\text{Na}_2\text{H}_4[\text{P}_2\text{W}_{17}\text{O}_{61}]\}$	2-	2144.87	2144.75
$\{\text{K}_2\text{Na}_4\text{H}_2[\text{P}_2\text{W}_{17}\text{O}_{61}]\}$	2-	2167.35	2167.24
$\{\text{K}_5\text{Na}_2\text{H}[\text{P}_2\text{W}_{17}\text{O}_{61}]\}$	2-	2191.81	2191.71
$\{\text{K}_5\text{NaH}_2[\text{P}_2\text{W}_{17}\text{O}_{61}]\}$	2-	2202.85	2202.74
$\{\text{K}_2\text{Na}_4\text{H}_2[\text{P}_2\text{W}_{17}\text{O}_{61}]\}$	2-	2205.80	2205.71
$\{\text{K}_6\text{NaH}[\text{P}_2\text{W}_{17}\text{O}_{61}]\}$	2-	2210.79	2210.70
$\{\text{K}_5\text{Na}_3[\text{P}_2\text{W}_{17}\text{O}_{61}]\}$	2-	2213.79	2213.72
$\{\text{K}_7\text{H}[\text{P}_2\text{W}_{17}\text{O}_{61}]\}$	2-	2218.78	2218.71
$\{\text{K}_6\text{Na}_2[\text{P}_2\text{W}_{17}\text{O}_{61}]\}$	2-	2221.78	2221.73
$\{\text{K}_8[\text{P}_2\text{W}_{17}\text{O}_{61}]\}$	2-	2237.75	2237.70
$\{\text{NaH}_{17}[\text{C}_{26}\text{H}_{12}\text{O}_{10}\text{N}_2\text{P}_2]_5\}$	2-	1455.55	1455.58
$\{\text{Na}_2\text{H}_{16}[\text{C}_{26}\text{H}_{12}\text{O}_{10}\text{N}_2\text{P}_2]_5\}$	2-	1466.54	1466.56

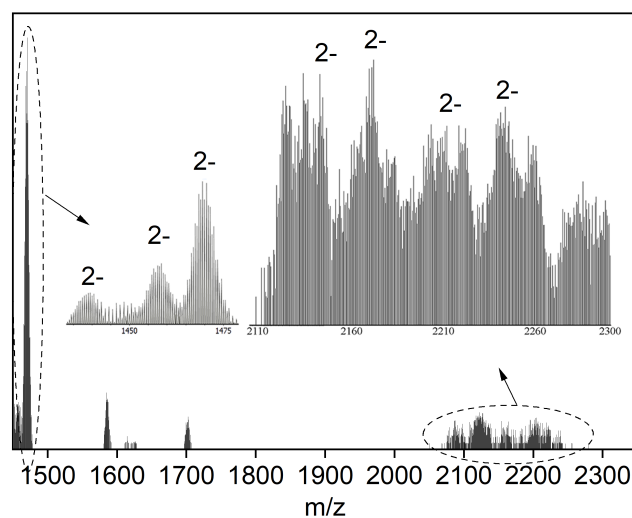


Figure 3.10: Negative mode ESI-MS spectrum of compound **I** in the m/z range 1400 - 2300

Interestingly, the result of CHN elemental analysis did not match the potassium salt of the hybrid POM. This has also been seen in the previous work in our group^[72]. As an

explanation, in the presence of HCl hydrolysis occurs of the acyl-N bond found in the dimethylacetamide solvent :



We considered that the cation may have been substituted by dimethylammonium (DMA^+), which should not be able to form bonds with phosphate anion at the end of **PMPDI** component, therefore the maximum DMA^+ bonded to the hybrid POM should be 6 which is the charge of the POM core. The CHN result matches this DMA salt of the product $([\text{C}_2\text{H}_6\text{N}]_6\text{H}_4[\text{P}_2\text{W}_{17}\text{O}_{61}((\text{P}=\text{O})\text{C}_{26}\text{H}_{12}\text{O}_7\text{N}_2\text{P})_2] \cdot 14 \text{H}_2\text{O})$ (Table 3.6), where the terminal phosphonic acids on the **PMPDI** ligands remain protonated.

Table 3.6: Result obtained for CHN elemental analysis of compound **I** compared to the predicted values

	%C	%H	%N
Predicted	13.03	1.64	2.37
Observed	12.81	1.74	2.85
	13.31	1.82	3

FT-IR was also used to confirm the composition of the product. Compared to the FT-IR spectra of **P₂W₁₇** and **PMPDI** (Figure 3.11), that of compound **I** has both the peaks for organic ligand (757.36 cm^{-1} for C–H in 2-disubstituted benzene derivative, 1269.81 and 1323.33 cm^{-1} for C–N in aromatic amine, 1376.84 cm^{-1} for O–H in phenol, 1415.94 cm^{-1} for O–H in carboxylic acid, 1677.31 cm^{-1} for C=O in conjugated ketone, 1718.47 cm^{-1} for C=O in carboxylic acid, 1771 1780 cm^{-1} for C=O in phenyl ester) and POM feature bonds (800 cm^{-1} for W–O–W, 989.92 cm^{-1} for P–O–W, 1121.64 for P=O).

The compound **I** dissolves well in neutral and acidic aqueous solutions with a red colour, but it has poor solubility in organic solvents such as acetonitrile, dimethyl sulfoxide (DMSO) and dimethylformamide (DMF), and displays a green colour in these solvents. As water is not an especially good solvent for cyclic voltammetry for its narrow potential windows of stability^[73], and is neither the best solvent for NMR, MS and UV-vis, we set up a cation exchange experiment to obtain a TBA salt of the PMPDI-POM

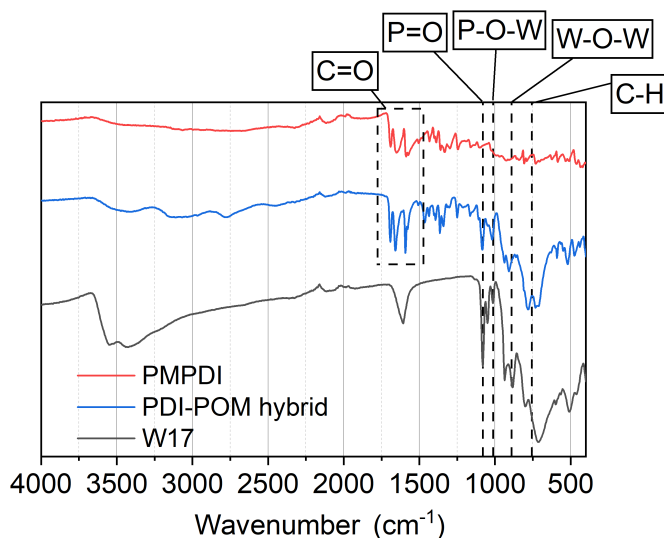


Figure 3.11: FT-IR spectra of **I** compared with the P_2W_{17} and PMPDI starting materials.

hybrid. The reaction was performed with 1 eq. of compound **I** mixed with 100 eq. TBA-Br in water acidified by 10 eq. HCl. Then the precipitate formed by this reaction was collected by centrifugation and washed by ethanol giving a dark red powder ($[\text{C}_{16}\text{H}_{36}\text{N}]_{10}[\text{P}_2\text{W}_{17}\text{O}_{61}((\text{P}=\text{O})\text{C}_{26}\text{H}_{12}\text{O}_7\text{N}_2\text{P})_2]$, compound **II**). However, the yield was low and after the precipitation, the solution was still deep red, which suggested the extent of reaction was low.

Compound **II** was characterised by ^{31}P NMR. There is only one peak at $\delta/\text{ppm} = -13.48$ in D_2O or $\delta/\text{ppm} = -13.22$ in CD_3CN (Figure 3.12), which is close to that expected for P_2W_{18} . The signal to noise ratio in D_2O is lower than that in CD_3CN due to the better solubility of compound **II** in organic solvents. However, the colour of compound **II** is deep red, suggesting some PDI remains inside but we could not observe any peaks in the NMR spectrum for the ligand. As PMPDI is negatively charged, it cannot form a typical class I hybrid such as those formed between dye cations and the POM anion.

FT-IR was also employed to characterize the resulting product. Compared to compound **I**, the IR spectrum of compound **II** is very similar with PMPDI and POM peaks and it has very weak TBA characteristic peaks at 2943.01 and 2870.98 cm^{-1} (Figure 3.13).

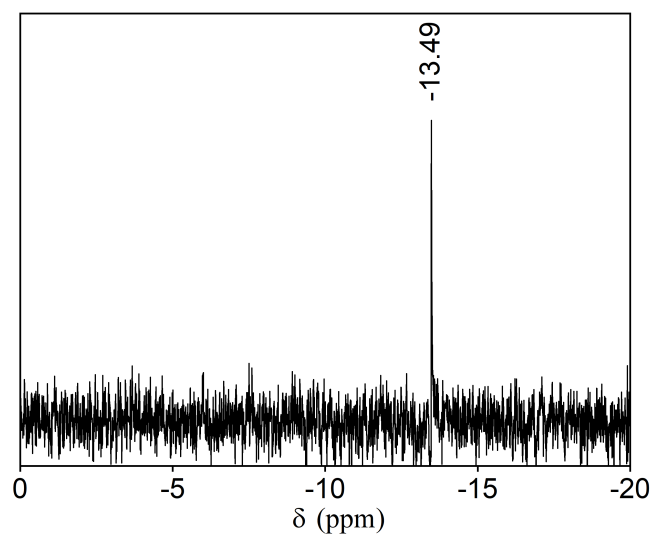


Figure 3.12: ^{31}P NMR spectra for compound **II** in D_2O .

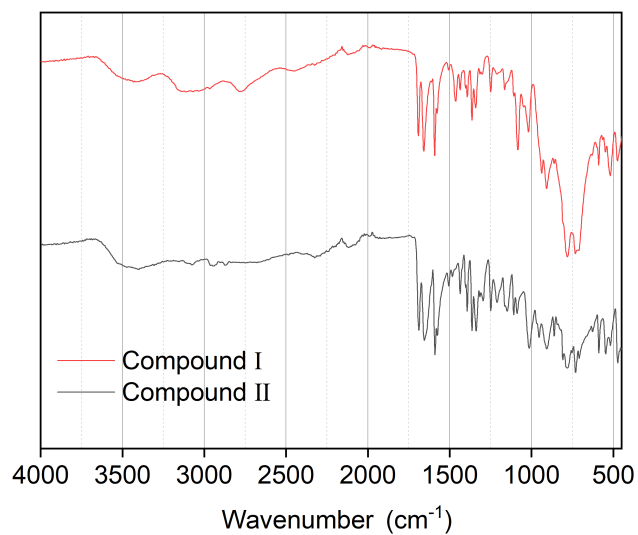


Figure 3.13: FT-IR spectra of compound **I** and compound **II**

Unfortunately, we were unable to characterise the **II** further and if so the purity could not be guaranteed, we decided not to proceed with the use of compound **II** in further CV, UV-vis and fluorometry analysis.

3.4 Electro- and Photo-Chemistry of The Hybrid POM

The redox character of $\mathbf{P}_2\mathbf{W}_{18}$ was probed by cyclic voltammetry. Although our product anion should have the same negative charge as $\mathbf{P}_2\mathbf{W}_{17}$ anion, the lacunary site of the $\mathbf{P}_2\mathbf{W}_{17}$ cluster will be occupied and the additional charges are from the phosphate group. Therefore the redox behaviour of the product is expected to be much more similar to $\mathbf{P}_2\mathbf{W}_{18}$. DMSO, DMF and acetonitrile are suitable solvents for POMs with their ability to dissolve such chemicals and their derivatives. Besides, the multiple redox processes of POMs result in negative region which usually fall within the wide electrochemical windows of these solvents^[73]. However, due to the bad solubility of **PMPDI** and compound **I** in these solvents, we had to use water as CV solvent with 0.1 M H_2SO_4 as electrolyte. During the initial testing the solvent encountered issue of being oxidized for the potential went beyond the solvent window, so we set the low voltage to -0.7 V (vs. Ag/AgCl). As shown in Figure 3.14, under different scan rates for three cycles, there was no significant anodic peak to cathodic peak separation (ΔE) to all the four segments, which means the reduction process is reversible both chemically and electrochemically^[74]. We used the scan rate $v = 0.1$ V/s to calculate $E_{1/2}$ and peak currents (I_p). The $E_{1/2}$ for the four quasi-reversible peaks are 28 mV, -139 mV, -401 mV and -642 mV vs. Ag/AgCl with the ratio of (I_p) $1 e^- : 1 e^- : 2 e^- : 2 e^-$, which showed the reversible redox process typical of $\mathbf{P}_2\mathbf{W}_{18}$.

CV was also run for **PMPDI**. The solubility for **PMPDI** in water increases with increasing pH, so the electrolyte was changed to 0.1 M KOH first. However, the cyclic voltammogram under these conditions was found to be featureless. Argon was used to degas the electrolyte solution to get rid of O_2 as the reduced **PMPDI** can be irreversibly oxidised by O_2 ^[75], but the result didn't change. Then we changed the solution to a pH 10 sodium carbonate buffer, which gave a clear cyclic voltammogram (Figure 3.15) of **PMPDI**. There are two segments for the irreversible redox process, with the $E_{1/2} = -24$ mV and -78 mV vs. Ag/AgCl, which fitted the nature of PDI as it is typical to see two

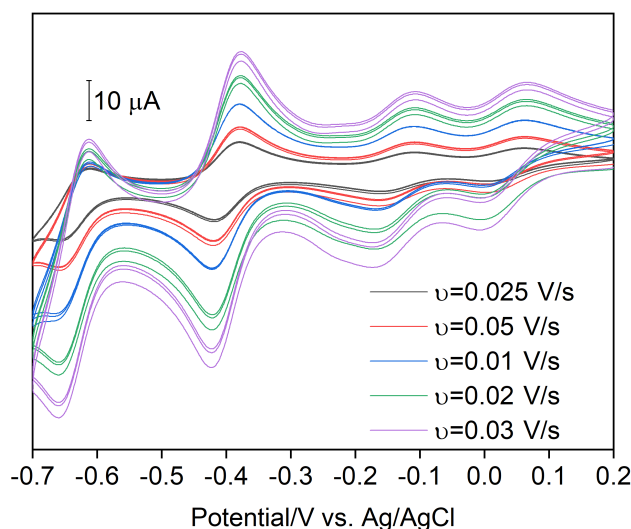


Figure 3.14: Cyclic voltammograms of a 1 mM aqueous solution of P_2W_{18} with five different scan rates

reduction waves in PDI dyes^[76].

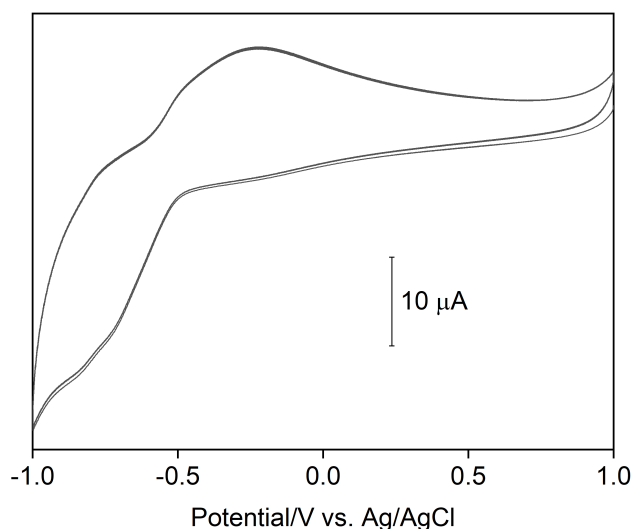


Figure 3.15: Cyclic voltammograms of a 1 mM aqueous solution of **PMPDI** with the scan rate $v = 0.1 \text{ V/s}$

CV voltammetry was then performed on compound **I** in 0.1 M H_2SO_4 aqueous solution under a positive pressure of Ar. The result shows four quasi-reversible peaks ($2 e^- : 3 e^- : 6 e^- : 4 e^-$) with little peak-to-peak separation under different scan rates (Figure 3.16). The $E_{1/2}$ calculated from the scan rate $v = 0.1 \text{ V/s}$ are 315 mV, -218 mV, -417 mV and -630 mV. Compared to P_2W_{18} , the $E_{1/2}$ values are positively shifted (Figure 3.17), as a result of electrochemical effects of organic groups containing positively charged P grafted

on to POMs^[77,78]. It is notable that there is a very sharp peak at -329 mV when oxidising the reduced compound **I**, which may suggest an irreversible electrode deposition process.

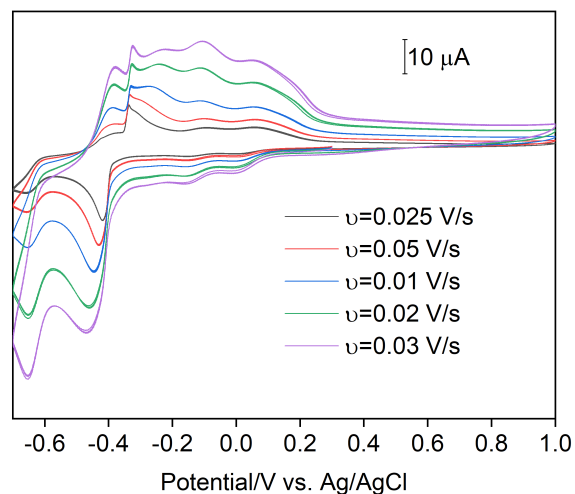


Figure 3.16: Cyclic voltammograms of a 1 mM aqueous solution of compound **I** with five different scan rates

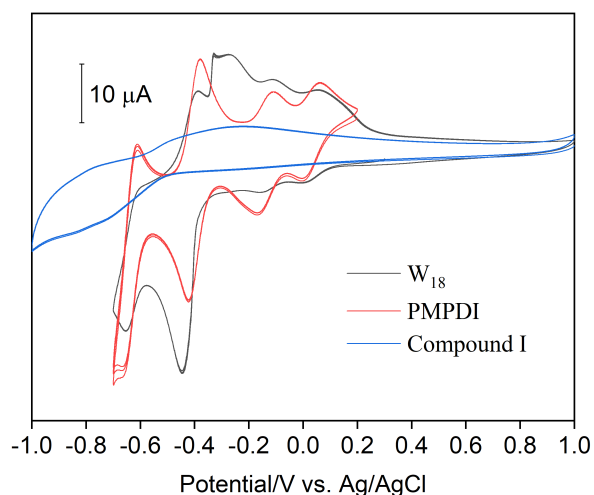


Figure 3.17: Cyclic voltammograms of P_2W_{18} (black), PMPDI (blue) and compound **I** (red)

The absorption properties of the hybrid was probed by UV-vis spectroscopy. The photoactivity of POM is restricted by the LMCT band energy to fall within the UV region of the spectrum. For P_2W_{18} and P_2W_{17} , the absorptions happen at wavelengths lower than 400 nm. There is a broad absorption for PMPDI at 498 nm, and also three shoulders at 598 nm, 542 nm and 480 nm. For the compound **I**, an absorption is also observed at

498nm with two shoulders at 534 nm and 470 nm (Figure 3.18), which demonstrates the generation of our visible light-sensitive hybrid-POM. It is possible that the extra shoulder seen from **PMPDI** at 598 nm is caused by the π -stacking aggregation between neighbouring perylene bisimides, which cannot happen in compound **I**, due to the steric effects of the POM^[79]. That may also partially be the reason for the better solubility of compound **I** than **PMPDI**. As there are two PDI ligands in the hybrid POM molecule but the absorption intensities of hybrid POM and **PMPDI** are quite close, this might suggest rapid charge transfer from visible light-excited **PMPDI** to the POM core.

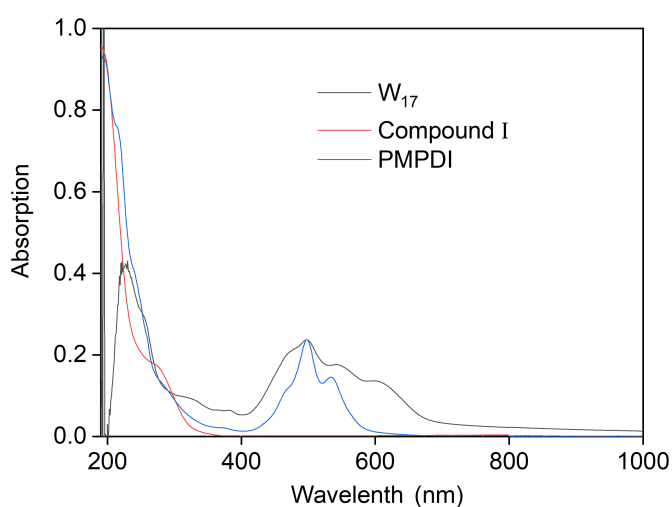


Figure 3.18: UV-vis spectra of P_2W_{17} , **PMPDI** and compound **I** in water (1×10^{-5} M)

It is notable that although both **PMPDI** and compound **I** have poor solubility in organic solvents, the color change from red in aqueous solutions to green in organic solutions is quite interesting. A very broad but weak absorption from 400 nm to 750 nm for the hybrid POM can be observed in DMF (Figure 3.19). A similar effect has been reported in the literature for N,N'-bis(2-phosphonoethyl)-3,4,9,10-perylenediimide (PPDI) showing pronounced spectrum changes in water and alcohol^[69]. The reason is that the dye molecules have a higher aggregation state in organic solvents^[80]. However, as mentioned above the π -stacking aggregation is much weaker in compound **I**, and correspondingly the absorption profile did not change as dramatically as that in **PMPDI**.

To explore whether there is charge transfer from the **PMPDI** ligand to the POM core

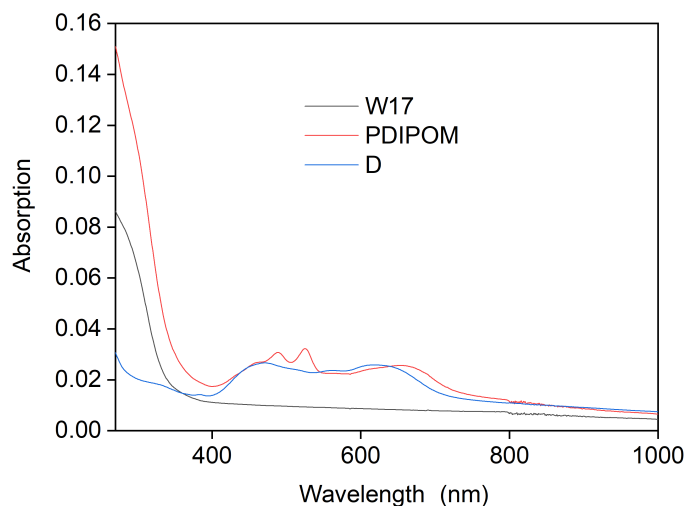


Figure 3.19: UV-vis spectra of P_2W_{17} , **PMPDI** and compound **I** in DMF (1×10^{-5} M)

in the hybrid compound **I**, fluorescence emission spectroscopy was used to explore the fluorescence behaviour. From the UV-vis spectroscopy, the maximum absorption of both the compound **I** and **PMPDI** happens at 498 nm and this was selected as the excitation wavelength. The emission spectrum of both compounds shows that **PMPDI** is strongly fluorescent in water with emission wavelengths at 545 nm (1.48×10^6 cps) and 586 nm (8.54×10^5 cps), whilst compound **I** shows similar features at 547 nm (4.75×10^5 cps) and 588 nm (4.01×10^5 cps) though with much weaker emission. If normalised by the number of **PMPDI** molecules per mole of compound, the emission intensities for the compound **I** are reduced by 83.95% and 76.52% respectively (Figure 3.20), which suggests effective intramolecular charge transfer from the excited photoactive ligand to the inorganic POM core, quenching the emission. However, there is no significant redshift of the emission wavelengths, which means the perylene planes and the methylene groups are not much twisted during the bonds vibration of the charge transfer.

To explore the photocatalytic properties of the hybrid POM, benzyl alcohol was employed as a substrate in combination the compound **I**. As compound **I** has poor solubility in acetonitrile and DMSO, we selected D_2O as solvent which allows easy NMR measurement of the reaction progress. Benzyl alcohol was selected as a suitable substrate due to its stronger reducibility than water^[81]. The benzyl alcohol was dissolved in D_2O with compound **I** as treatment group, and solutions with the same concentration of benzyl alcohol

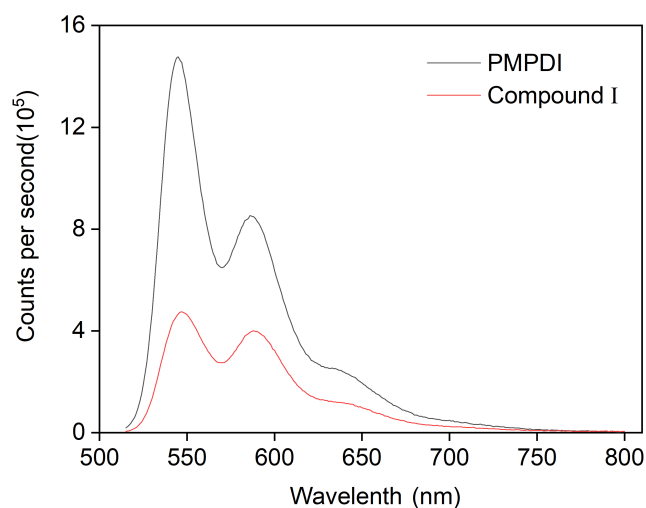


Figure 3.20: Fluorescence emission spectrum of **PMPDI** compared to compound **I** normalised by the molarity of fluorescent chromophore species. Excitation wavelength = 498 nm.

only and benzyl alcohol with PDI were the control groups. The wavelength of irradiation was filtered to > 455 nm using a UV cut-off filter to avoid direct excitation of the POM core. After 18 hours of irradiation, the signal of the proton peak of the phenyl hydroxyl decreased by 2.27% (which is not outside a reasonable margin of error), whilst no change for that of control groups was observed (Figure 3.21). It may be that the reaction is one-way, with conversion related to the dosage of compound **I** as the molarity of it is 1 percent versus benzyl alcohol.

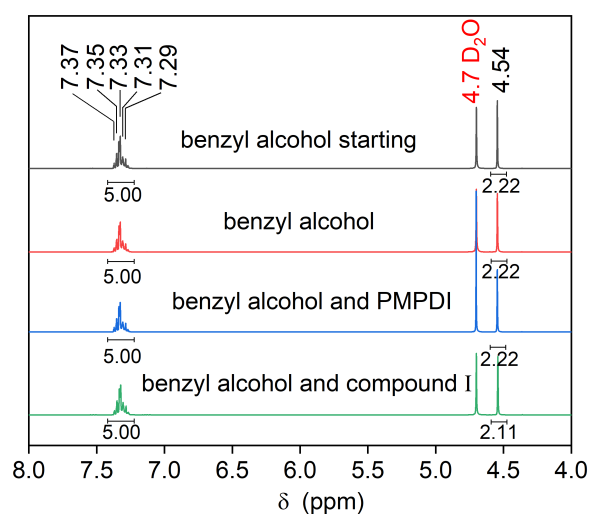


Figure 3.21: ¹H NMR result of benzyl alcohol photo-oxidation

To explore this, we set up another treatment group with the ratio of compound **I** increased by 10 times, and the result was effectively the same (Figure 3.22). We chose D₂O for easy NMR measurement, however, the solubility of benzyl alcohol in D₂O is low^[82], and during the photocatalytic reaction, D₂O does not have the ability to stabilise reaction via solvation or inhibit proton transfer^[83]. Therefore, D₂O is not the appropriate solvent for this reaction. Moreover, lacking of temperature control under long-term high power irradiation might also cause the loss of product.

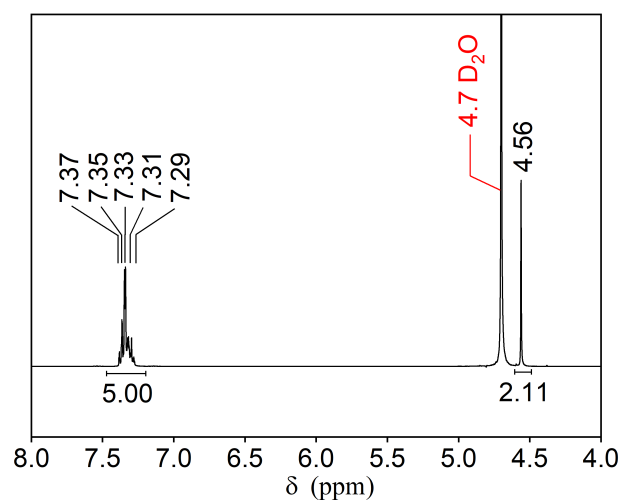


Figure 3.22: ¹H NMR result of benzyl alcohol photo-oxidation with the ratio of compound **I** increased by 10 times

4 Conclusion and Further Work

In conclusion, a new post-functionalised hybrid polyoxometalate based on a mono-lacunary Wells-Dawson cluster was synthesised using an organic chromophore, **PMPDI**, as a covalently grafted moiety. The as synthesised POM was structurally confirmed by ^{31}P NMR, Mass Spectrometry and other characterisation. Electrochemical analysis confirms that, it has reversible redox processes at suitable potentials. According to UV-vis spectrometry, the hybrid POM has a strong absorption at 498 nm which falls in the visible light region of the spectrum. Moreover, intermolecular charge transfer from the organic component to the POM core was also confirmed by fluorimetry. The as synthesised product was used as catalyst for the photooxidation of benzyl alcohol, but the initial test was not successful due to the inappropriate solvent and lacking of temperature control.

To take this project further, it would be worth trying to adjust the reactant and reaction conditions to improve the redox properties of our hybrid POM. The (aminomethyl)-phosphonic acid used for **PMPDI** synthesis may be replaced with phosphanilic acid or 2-(aminoethyl)phosphonic acid to grow carbon chain to reduce steric hindrance. Crystallisation plays an important role in POM synthesis. However, both evaporation and slow diffusion in ethanol gave fine powder instead of crystal of our product. In future work, appropriate solvent and method should be explored for crystallisation and some crystallography characterisation will be applied. Suitable methods would be explored for cation exchange to improve the solubility of hybrid POM in organic solvents, so that better flexibility of NMR and CV can be achieved, and there will be more choices for photocatalytic conditions. For the photooxidation part, the oxide O_2 might be changed to other oxy-

gen source such as hydrogen peroxide. It may also be necessary to try different reactant ratios and reaction conditions to make polymers as both **PMPDI** and **P₂W₁₇** are symmetrical in structure. Further more, photo-polymerisable ionic liquid (PIL) matrix that can stabilise the hybrid POM and allow its processing through additive manufacturing (3D printing) may be applied. This will translate our molecular component to tangible macroscopic objects to develop novel materials for catalysis.

5 Experimental

5.1 Materials and Instrumentation

All commercially available reagents and solvents are purchased from Sigma Aldrich Corporation, Alfa Aesar or Thermo Fisher Scientific, without further purification before used.

Nuclear Magnetic Resonance (NMR) spectroscopy experiments was performed on a Bruker AV400 spectrometer at 298 K. Chemical shifts (δ) are recorded in parts per million (ppm).

Electrospray Ionisation Mass Spectrometry (ESI-MS) experiments was performed on a Bruker micro-TOF II mass spectrometer. The instrument parameters was adapted for the detection of negative polyoxometalate anions with high molecular weight. Samples were introduced to the spectrometer under automation through mixing with a stream of MeOH : H₂O (70 : 30 V/V).

CHN Elemental Microanalysis was performed on an Exeter analytical CE-440 Elemental Analyzer by the University of Nottingham School of Chemistry elemental microanalysis service.

Attenuated Total Reflection Fourier-transform Infra-red spectroscopy (ATR-FTIR) experiments were performed on a Bruker Tensor 27 spectrometer equipped with a Pike GladiATR module with a diamond crystal.

UV-vis spectroscopy (UV-vis) experiments were performed on an Agilent Cary 5000 UV-

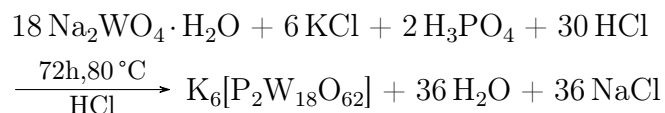
Vis-NIR Absorption spectrometer using the standard double cuvette holder module in absorption mode.

Fluorescence spectrometry experiment was performed on an Edinburgh Instruments FLS980 Photoluminescence spectrometer with the excitation wavelength of 498nm.

Cyclic Voltammetry (CV) was performed on a CHI600E workstation for solution state measurements. It is a standard three electrode set-up, the working electrode is a glassy carbon electrode ($d = 3$ mm), the counter electrode is Pt wire and a Ag/AgCl electrode works as reference electrode.

5.2 Synthesis

5.2.1 $\text{K}_6[\text{P}_2\text{W}_{18}\text{O}_{62}]$ (P_2W_{18})



This synthesis was conducted as reported by Graham and Finke^[84].

In a 500mL round-bottom flask, sodium tungstate dihydrate ($\text{Na}_2\text{WO}_4 \cdot \text{H}_2\text{O}$) (60 g, 192.8 mmol) was dissolved in H_2O (70 mL) with vigorous stirring. After the solution became clear and colorless, HCl (4 M, 50 mL) was added to the solution in a dropping funnel at the rate of 2 drops per second. White precipitation forms and the solution became cloudy, then became clear again under stirring. H_3PO_4 (4 M, 50 mL) was added at the rate of 4 drops per second in the same way during which the color of the solution changed to yellow. Then temperature was raised to 110°C and the whole system was heated to boiling with a condenser on the flask. The refluxing lasted 24 hours in dark covered with foil.

As the solution was cooled down to room temperature on the bench top, it was transferred

into a 500 mL beaker, and KCl (30 g) was added slowly in 20 seconds while stirring, forming yellow precipitate. The solution was stirred for another 10mins to precipitate completely. The mixture was then filtered with a porosity glass funnel, and the solid was air dried overnight. The dried material was collected and dissolved in 65mL deionized water while stirring and heating (80 °C). Six drops of liquid bromine was added to oxidize the tungsten, resulting in the color changing from green to yellow. The solution was transferred to a 150 mL beaker and evaporated 3 days covered with foil to give bright yellow crystals. Yield : 22.7 g, 4.94 mmol, 46.12%. ^{31}P NMR (162 MHz, $\text{D}_2\text{O-d}_2$) : $\delta/\text{ppm} = -13.02$; ATR-FTIR $\nu_{\text{max}} / \text{cm}^{-1}$: 1697.89 (H_2O), 1162.80, 1037.26 and 1012.56 (P-O), 940.53 (W=O), 858.21 (W-O-W).

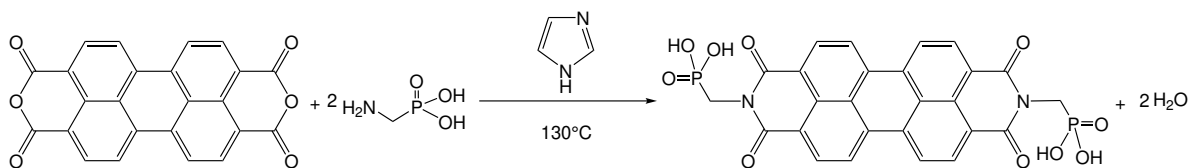
5.2.2 $\alpha\text{-K}_{10}[\text{P}_2\text{W}_{17}\text{O}_{61}] \cdot 20\text{H}_2\text{O}$ (P_2W_{17})



This synthesis was conducted as reported in Inorganic Syntheses, Volume 27^[68].

In a 250 mL beaker, a sample of α - or β - $\text{K}_6[\text{P}_2\text{W}_{18}\text{O}_{62}] \cdot x\text{H}_2\text{O}$ (16 g, 2.3×10^{-3} mol) was dissolved in 40 mL H_2O . An aqueous solution of KHCO_3 (1.782 mol/L, 40 mL) was added to the same beaker whilst stirring resulting in a milky suspension. It took an hour to finish the reaction and the white precipitation was collected and dried on a coarse sintered glass frit under suction. Recrystallization in water was employed to give chalky crystalline powder. Yield : 12.11 g, 74.36%. ^{31}P NMR (162 MHz, $\text{D}_2\text{O-d}_2$) : $\delta/\text{ppm} = -7.22, -14.36$; ATR-FTIR $\nu_{\text{max}} / \text{cm}^{-1}$: 1708.18 (H_2O), 1166.92, 1064.01 and 1029.03 (P-O), 996.10 (W=O), 856.14 (W-O-W).

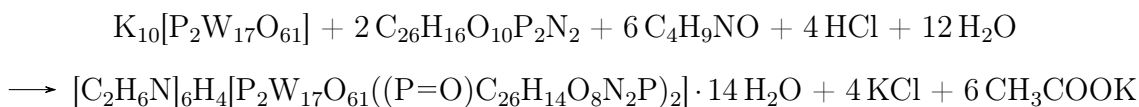
5.2.3 C₂₆H₁₆O₁₀P₂N₂ (PMPDI)



This synthesis was conducted as reported by Kirner et al.^[67]. In a 50 mL round-bottom flask equipped with a side-arm, perylene-3,4,9,10-tetracarboxylic dianhydride (PTCDA) (158 mg, 0.4 mmol), (aminomethyl)-phosphonic acid (94 mg, 0.84 mmol) and imidazole (3 g) was added whilst stirring, making evenly mixed red powder. The flask was then sealed with a rubber plug and heated to 130°C, during which a needle was employed to let out the air twice preventing excessive pressure inside the flask. From when the imidazole acting as solvent melted completely, the system was heated for 20 minutes and the color got deeper, after which the flask was cooled down in air. A solution of ethanol : HCl (2 M) = 1:1 (volume) was added to the mixture making black precipitate. The solid was collected via vacuum filtering and washed by 10mL solution of ethanol : H₂O =1:1 (volume) then 10mL ethanol, after what suspended in 20 mL DI water in a beaker which was monitored by a pH meter. The pH was slowly brought to 8.9 by dropwise of KOH solution (1 M) to dissolve the product and not too basic so that the possibly unreacted PTCDA would not dissolve. With the addition of dropwise of HCl (2 M) to filtrate from the above-mentioned mixture and rapid magnetic stirring, a red gel slowly formed from pH 5 until pH 1, and then collected by vacuum suction. In order not to introduce fibre from the filter paper into the product, the gel was removed before it gets too dry and then dried overnight in a vacuum dryer. The final product was extremely thin slice that it can float easily in air with even slight movement. Yield : 193 mg, 83.4% ¹H NMR (400 MHz, D₂O-d₂) : δ/ppm = 7.92 (8H), 4.20 (4H); ³¹P NMR (162 MHz, D₂O-d₂) : δ/ppm = 12.17; TR-FTIR v_{\max} / cm⁻¹ : 3066 cm⁻¹ br w, 2996 w, 2319 w, 2113 w, 1990 w, 1887 w, 1689 s, 1650 s, 1586 s, 1504 w, 1432 m, 1389 m, 1333 m, 1245 m, 1160 w, 1098 w, 924 m, 841 w, 806 w, 732 w, 623 w, 586 w, 533 w; CHN % : C 49.1 and 49.28, H 2.9 and 2.82,

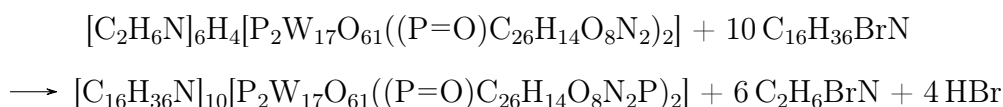
N 5.1 and 5.01.

5.2.4 $[\text{C}_2\text{H}_6\text{N}]_6\text{H}_4[\text{P}_2\text{W}_{17}\text{O}_{61}((\text{P}=\text{O})\text{C}_{26}\text{H}_{12}\text{O}_7\text{N}_2\text{P})_2] \cdot 14 \text{H}_2\text{O}$ (I)



$\text{K}_{10}[\text{P}_2\text{W}_{17}\text{O}_{61}]$ (227.7 mg, 0.05 mmol) was suspended in 10 mL N,N-Dimethylacetamide (DMA) and 5 mL water in a 25 mL round-bottomed flask whilst stirring. Then KCl (30.12 mg) and **PMPDI** (52 mg, 0.1 mmol) was dissolved in the solvent. The suspension turned into clear red solution with HCl (12 M, 83 μL) added. The system was heated to 130 °C while refluxing with a condenser on top of the flask. After 24 hours of reaction the solution was allowed to cool down to room temperature and filtered subsequently to remove possible excess reactants. In a 250 mL beaker, the solution was tardily added into 60mL ether under stirring and some green solid separated out. The precipitation was collected by centrifuging and washed with ether, ethanol and ether successively before it was air dried in dark. Yield : 258.12 mg, 4.9%. ^{31}P NMR (162 MHz, $\text{D}_2\text{O}-d_2$) : $\delta/\text{ppm} = 13.94, -7.49, -13.03, -14.25$; TR-FTIR $\nu_{\text{max}} / \text{cm}^{-1}$: 732.67 (W–O–W), 907.60 (P–O–W), 1018.73 (P=O), 1212.19 and 1249.43 (C–N), 1364.49 and 1393.30 (O–H), 1590.87, 1658.79, 1691.72 (C=O); CHN % : C 12.81 and 13.31, H 1.74 and 1.82, N 2.85 and 3.

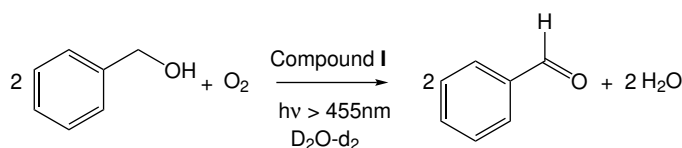
5.2.5 $[\text{C}_{16}\text{H}_{36}\text{N}]_{10}[\text{P}_2\text{W}_{17}\text{O}_{61}((\text{P}=\text{O})\text{C}_{26}\text{H}_{12}\text{O}_7\text{N}_2\text{P})_2]$ (II)



In a glass vial, Tetra-n-butylammonium bromide (TBA Br, 322 mg, 1 mmol) was dissolved in 2 mL water and acidified by 2.5 μL 4 M HCl, then 5 mL aqueous solution of PDI-POM

hybrid (52 mg) was tardily added into it by dropwise while stirring. After two hours, the red suspension was poured into 40 mL ethanol, followed by centrifugation. The precipitation was washed twice with ethanol, then vacuum dried overnight. Yield : 5.7 mg, 10.9%. ^{31}P NMR (162 MHz, $\text{CD}_3\text{CN-d}_3$) : $\delta/\text{ppm} = 13.22$; TR-FTIR $\nu_{\text{max}} / \text{cm}^{-1}$: 2943.01, 2870.98, 1687.60, 1594.99, 1393.30, 1014.62, 907.60, 782.06, 588.60.

5.3 Benzyl Alcohol Photo-Oxidation



This method was conducted as reported by Zhang et al.^[81].

Three solutions are prepared in microwave tubes with stirring bar :

1. benzyl alcohol (103.6 μL , 1 mmol) in 5 mL D_2O
2. benzyl alcohol (103.6 μL , 1 mmol) and **PMPDI** (6.2 mg, 10 μmol) in 5 mL D_2O
3. benzyl alcohol (103.6 μL , 1 mmol) and compound **I** (60 mg, 10 μmol) in 5 mL D_2O

^1H NMR (400 MHz, $\text{D}_2\text{O-d}_2$) are measured for three solutions. Afterwards the microwave tubes were sealed and oxygenated by a long needle inserted with a shorter needle to balance pressure respectively for 10 minutes. The top of the tubes were filled with oxygen with the pressure of 5 bar. The microwave tubes were subsequently irradiated while stirring in a photo-reactor with a 200 W Xe lamp with a UV cut-off filter for 18 hours. Then ^1H NMR (400 MHz, $\text{D}_2\text{O-d}_2$) data was collected again.

Bibliography

- [1] Dolbecq, A., Dumas, E., Mayer, C. R. & Mialane, P. Hybrid organic-inorganic polyoxometalate compounds: From structural diversity to applications. *Chemical Reviews* **110**, 6009–6048 (2010).
- [2] Long, D. L., Tsunashima, R. & Cronin, L. Polyoxometalates: Building blocks for functional nanoscale systems. *Angewandte Chemie International Edition* **49**, 1736–1758 (2010).
- [3] Du, D. Y., Qin, J. S., Li, S. L., Su, Z. M. & Lan, Y. Q. Recent advances in porous polyoxometalate-based metal-organic framework materials. *Chemical Society Reviews* **43**, 4615–4632 (2014).
- [4] Liu, R. *et al.* Enhanced proton and electron reservoir abilities of polyoxometalate grafted on graphene for high-performance hydrogen evolution. *Energy & Environmental Science* **9**, 1012–1023 (2016).
- [5] Wang, S. S. & Yang, G. Y. Recent advances in polyoxometalate-catalyzed reactions. *Chemical Reviews* **115**, 4893–4962 (2015).
- [6] Walsh, J. J., Bond, A. M., Forster, R. J. & Keyes, T. E. Hybrid polyoxometalate materials for photo(electro-) chemical applications. *Coordination Chemistry Reviews* **306**, 217–234 (2016).
- [7] Proust, A. *et al.* Functionalization and post-functionalization: A step towards polyoxometalate-based materials. *Chemical Society Reviews* **41**, 7605–7622 (2012).

- [8] Baker, L. C. & Glick, D. C. Present general status of understanding of heteropoly electrolytes and a tracing of some major highlights in the history of their elucidation. *Chemical Reviews* **98**, 3–50 (1998).
- [9] Lipscomb, W. N. Paratungstate ion. *Inorganic Chemistry* **4**, 132–134 (1965).
- [10] Pope, M. T. Heteropoly and isopoly anions as oxo complexes and their reducibility to mixed-valence blues. *Inorganic Chemistry* **11**, 1973–1974 (1972).
- [11] Pope, M. T. & Müller, A. Polyoxometalate chemistry: An old field with new dimensions in several disciplines. *Angewandte Chemie International Edition in English* **30**, 34–48 (1991).
- [12] Poblet, J. M., López, X. & Bo, C. Ab initio and DFT modelling of complex materials: Towards the understanding of electronic and magnetic properties of polyoxometalates. *Chemical Society Reviews* **32**, 297–308 (2003).
- [13] Pope, M. T. Heteropoly and isopoly oxometalates. *Inorganic Chemistry Concepts* **8** (1983).
- [14] Pope, M. T. Inorganic chemistry concepts. *Heteropoly and Isopoly Oxometalates* (1983).
- [15] Yang, H. *et al.* pH-Dependent syntheses and crystal structures of a series of organic-inorganic hybrids constructed from Keggin or Wells-Dawson polyoxometalates and silver coordination compounds. *Inorganic Chemistry* **49**, 736–744 (2010).
- [16] Hayashi, Y. Hetero and lacunary polyoxovanadate chemistry: Synthesis, reactivity and structural aspects. *Coordination Chemistry Reviews* **255**, 2270–2280 (2011).
- [17] Chen, L. *et al.* A basket tetradecavanadate cluster with blue luminescence. *Journal of the American Chemical Society* **127**, 8588–8589 (2005).
- [18] Kurata, T., Uehara, A., Hayashi, Y. & Isobe, K. Cyclic polyvanadates incorporating template transition metal cationic species: Synthesis and struc-

- tures of hexavanadate $[\text{PdV}_6\text{O}_{18}]^{4-}$, octavanadate $[\text{Cu}_2\text{V}_8\text{O}_{24}]^{4-}$, and decavanadate $[\text{Ni}_4\text{V}_{10}\text{O}_{30}(\text{OH})_2(\text{H}_2\text{O})_6]_4$. *Inorganic Chemistry* **44**, 2524–2530 (2005).
- [19] Dronskowski, R., Kikkawa, S. & Stein, A. *Handbook of Solid State Chemistry, 6 Volume Set* (John Wiley & Sons, 2017).
- [20] Cameron, J. M., Wales, D. J. & Newton, G. N. Shining a light on the photosensitisation of organic-inorganic hybrid polyoxometalates. *Dalton Transactions* **47**, 5120–5136 (2018).
- [21] Lindqvist, I. The structure of the tetramolybdate ion. *Arkiv För Kemi* **2**, 349–355 (1950).
- [22] Anderson, J. S. Constitution of the poly-acids. *Nature* **140**, 850–850 (1937).
- [23] Keggin, J. Structure of the crystals of 12-phosphotungstic acid. *Nature* **132**, 351–351 (1933).
- [24] Dawson, B. The structure of the 9(18)-heteropoly anion in potassium 9(18)-tungstophosphate, $\text{K}_6(\text{P}_2\text{W}_{18}\text{O}_{62}) \cdot 14 \text{H}_2\text{O}$. *Acta Crystallographica* **6**, 113–126 (1953).
- [25] Wells, A. F. *Structural inorganic chemistry* (Oxford University Press, 2012).
- [26] Coronado, E. & Gomez-Garcia, C. J. Polyoxometalate-based molecular materials. *Chemical Reviews* **98**, 273–296 (1998).
- [27] López, X., Bo, C. & Poblet, J. M. Electronic properties of polyoxometalates: Electron and proton affinity of mixed-addenda Keggin and Wells-Dawson anions. *Journal of the American Chemical Society* **124**, 12574–12582 (2002).
- [28] Zhang, F. Q. *et al.* On the origin of the relative stability of Wells–Dawson isomers: A DFT study of α -, β -, γ -, α^* -, β^* -, and γ^* - $[(\text{PO}_4)_2\text{W}_{18}\text{O}_{54}]^{6-}$ anions. *Inorganic Chemistry* **50**, 4967–4977 (2011).
- [29] Acerete, R., Hammer, C. F. & Baker, L. C. Reinterpretations, based on ^{183}W NMR spectra, of several heteropolytungstates derived from the Wells-Dawson "2 : 18"

- structure. Preparation and structure proof for the first γ -isomer of a 2 : 18 complex. *Inorganic Chemistry* **23**, 1478–1482 (1984).
- [30] Contant, R. & Thouvenot, R. A reinvestigation of isomerism in the Dawson structure: Syntheses and ^{183}W NMR structural characterization of three new polyoxotungstates $[\text{X}_2\text{W}_{18}\text{O}_{62}]^{6-}$ (X= P^{V} , As^{V}). *Inorganica Chimica Acta* **212**, 41–50 (1993).
- [31] Neubert, H. & Fuchs, J. Crystal structures and vibrational spectra of two isomers of octadecatungsto-diarsenate $(\text{NH}_4)_6\text{As}_2\text{W}_{18}\text{O}_{62} \cdot n\text{H}_2\text{O}$. *ChemInform* **18**, no–no (1987).
- [32] Maksimovskaya, R. & Maksimov, G. Identification of γ -isomer of heteropoly anion $\text{P}_2\text{W}_{18}\text{O}_{62}^{6-}$ by ^{31}P , ^{183}W , and ^{17}O NMR. *Zhurnal Neorganicheskoi Khimii* **40**, 1369–1371 (1995).
- [33] Richardt, P. J., Gable, R. W., Bond, A. M. & Wedd, A. G. Synthesis and redox characterization of the polyoxo anion, $\gamma^*-\text{[S}_2\text{W}_{18}\text{O}_{62}]^{4-}$: A unique fast oxidation pathway determines the characteristic reversible electrochemical behavior of polyoxometalate anions in acidic media. *Inorganic Chemistry* **40**, 703–709 (2001).
- [34] Yuan, M. *et al.* Modified polyoxometalates: Hydrothermal syntheses and crystal structures of three novel reduced and capped Keggin derivatives decorated by transition metal complexes. *Inorganic Chemistry* **42**, 3670–3676 (2003).
- [35] Hashikawa, A., Fujimoto, M., Hayashi, Y. & Miyasaka, H. Isolation of a stable lacunary Dawson-type polyoxomolybdate cluster. *Chemical Communications* **47**, 12361–12363 (2011).
- [36] Fang, X. & Hill, C. L. Multiple reversible protonation of polyoxoanion surfaces: Direct observation of dynamic structural effects from proton transfer. *Angewandte Chemie International Edition* **46**, 3877–3880 (2007).
- [37] Rocchiccioli-Deltcheff, C. & Thouvenot, R. Vibrational studies of heteropolyanions related to $\alpha\text{-P}_2\text{W}_{18}\text{O}_{62}^{6-}$ i-infrared evidence of the structure of α_1 and $\alpha_2\text{-P}_2\text{W}_{17}\text{O}_{61}^{10-}$. *Spectroscopy Letters* **12**, 127–138 (1979).

- [38] Finke, R. G. & Droege, M. W. Trivacant heteropolytungstate derivatives. 2. Synthesis, characterization, and ^{183}W NMR of $[\text{P}_4\text{W}_{30}\text{M}_4(\text{H}_2\text{O})_2\text{O}_{112}]^{16-}$ ($\text{M} = \text{Co}, \text{Cu}, \text{Zn}$). *Inorganic Chemistry* **22**, 1006–1008 (1983).
- [39] Massart, R., Contant, R., Fruchart, J. M., Ciabrini, J. P. & Fournier, M. Phosphorus-31 NMR studies on molybdic and tungstic heteropolyanions. Correlation between structure and chemical shift. *Inorganic Chemistry* **16**, 2916–2921 (1977).
- [40] Katsoulis, D. E. A survey of applications of polyoxometalates. *Chemical Reviews* **98**, 359–388 (1998).
- [41] Amatore, C. & Saveant, J. M. Mechanism and kinetic characteristics of the electrochemical reduction of carbon dioxide in media of low proton availability. *Journal of the American Chemical Society* **103**, 5021–5023 (1981).
- [42] López, X., Carbó, J. J., Bo, C. & Poblet, J. M. Structure, properties and reactivity of polyoxometalates: A theoretical perspective. *Chemical Society Reviews* **41**, 7537–7571 (2012).
- [43] Gumerova, N. I. & Rompel, A. Synthesis, structures and applications of electron-rich polyoxometalates. *Nature Reviews Chemistry* **2**, 1–20 (2018).
- [44] Maestre, J. M., Lopez, X., Bo, C., Poblet, J.-M. & Casan-Pastor, N. Electronic and magnetic properties of α -Keggin anions: A DFT study of $[\text{XM}_{12}\text{O}_{40}]^{n-}$, ($\text{M} = \text{W}, \text{Mo}$; $\text{X} = \text{Al}^{\text{III}}, \text{Si}^{\text{IV}}, \text{P}^{\text{V}}, \text{Fe}^{\text{III}}, \text{Co}^{\text{II}}, \text{Co}^{\text{III}}$) and $[\text{SiM}_{11}\text{VO}_{40}]^{m-}$ ($\text{M} = \text{Mo}$ and W). *Journal of the American Chemical Society* **123**, 3749–3758 (2001).
- [45] López, X., Fernández, J. A. & Poblet, J. M. Redox properties of polyoxometalates: New insights on the anion charge effect. *Dalton Transactions* 1162–1167 (2006).
- [46] Kastner, K. *et al.* Redox-active organic-inorganic hybrid polyoxometalate micelles. *Journal of Materials Chemistry A* **5**, 11577–11581 (2017).
- [47] Papaconstantinou, E. & Hiskia, A. Photochemistry and photocatalysis by polyoxometalates. In *Polyoxometalate Molecular Science*, 381–416 (Springer, 2003).

- [48] Lei, P. *et al.* Degradation of dye pollutants by immobilized polyoxometalate with H_2O_2 under visible-light irradiation. *Environmental Science & Technology* **39**, 8466–8474 (2005).
- [49] Tzirakis, M. D., Lykakis, I. N. & Orfanopoulos, M. Decatungstate as an efficient photocatalyst in organic chemistry. *Chemical Society Reviews* **38**, 2609–2621 (2009).
- [50] Gouzerh, P. & Proust, A. Main-group element, organic, and organometallic derivatives of polyoxometalates. *Chemical Reviews* **98**, 77–112 (1998).
- [51] Proust, A., Thouvenot, R. & Gouzerh, P. Functionalization of polyoxometalates: Towards advanced applications in catalysis and materials science. *Chemical Communications* 1837–1852 (2008).
- [52] Kibler, A. J. & Newton, G. N. Tuning the electronic structure of organic-inorganic hybrid polyoxometalates: The crucial role of the covalent linkage. *Polyhedron* **154**, 1–20 (2018).
- [53] Berardi, S., Carraro, M., Sartorel, A., Modugno, G. & Bonchio, M. Hybrid polyoxometalates: Merging organic and inorganic domains for enhanced catalysis and energy applications. *Israel Journal of Chemistry* **51**, 259–274 (2011).
- [54] Miras, H. N., Yan, J., Long, D. L. & Cronin, L. Engineering polyoxometalates with emergent properties. *Chemical Society Reviews* **41**, 7403–7430 (2012).
- [55] Hill, C. Polyoxometalates in catalysis. *Journal of Molecular Catalysis. A, Chemical* **262** (2007).
- [56] Bonchio, M. *et al.* Hierarchical organization of perylene bisimides and polyoxometalates for photo-assisted water oxidation. *Nature Chemistry* **11**, 146–153 (2019).
- [57] Poddutoori, P. K., Kandrashkin, Y. E., Obondi, C. O., D’Souza, F. & Van Der Est, A. Triplet electron transfer and spin polarization in a palladium porphyrin-fullerene conjugate. *Physical Chemistry Chemical Physics* **20**, 28223–28231 (2018).

- [58] Matt, B. *et al.* Charge photo-accumulation and photocatalytic hydrogen evolution under visible light at an iridium(III)-photosensitized polyoxotungstate. *Energy & Environmental Science* **6**, 1504–1508 (2013).
- [59] Jansen, S. A., Wang, S.-H. & Eddowes, A. D. Stability and acidity contributions of heteropolymetalates: A theoretical study of the Keggin and Dawson ions. *Supramolecular Science* **4**, 51–58 (1997).
- [60] Tian, A. X. *et al.* Assembly of the highest connectivity Wells-Dawson polyoxometalate coordination polymer: The use of organic ligand flexibility. *Inorganic Chemistry* **47**, 3274–3283 (2008).
- [61] Fournier, M. & Ginsberg, A. Inorganic synthesis. *John Wiley: New York* **27**, 80 (1990).
- [62] Smith, B. J. & Patrick, V. A. Quantitative determination of sodium metatungstate speciation by ^{183}W NMR spectroscopy. *Australian Journal of Chemistry* **53**, 965–970 (2000).
- [63] Canny, J., Teze, A., Thouvenot, R. & Herve, G. Disubstituted tungstosilicates. 1. synthesis, stability, and structure of the lacunary precursor polyanion of a tungstosilicate $\gamma\text{-}[\text{SiW}_{10}\text{O}_{36}]^{8-}$. *Inorganic Chemistry* **25**, 2114–2119 (1986).
- [64] Law, K. Y. Organic photoconductive materials: Recent trends and developments. *Chemical Reviews* **93**, 449–486 (1993).
- [65] Pasaogullari, N., Icil, H. & Demuth, M. Symmetrical and unsymmetrical perylene diimides: Their synthesis, photophysical and electrochemical properties. *Dyes and Pigments* **69**, 118–127 (2006).
- [66] Langhals, H. Cyclic carboxylic imide structures as structure elements of high stability. Novel developments in perylene dye chemistry. *Heterocycles* **1**, 477–500 (1995).
- [67] Kirner, J. T., Stracke, J. J., Gregg, B. A. & Finke, R. G. Visible-light-assisted photoelectrochemical water oxidation by thin films of a phosphonate-functionalized pery-

- lene diimide plus CoOx cocatalyst. *ACS Applied Materials & Interfaces* **6**, 13367–13377 (2014).
- [68] Contant, R., Klemperer, W. G. & Yaghi, O. Potassium octadecatungstodiphosphates(V) and related lacunary compounds. *Inorganic Syntheses* **27**, 104–111 (1990).
- [69] Marcon, R. O. & Brochsztain, S. Characterization of self-assembled thin films of zirconium phosphonate/aromatic diimides. *Thin Solid Films* **492**, 30–34 (2005).
- [70] Rodríguez Abreu, C., Aubery Torres, C., Solans, C., López Quintela, A. & Tiddy, G. J. Characterization of perylene diimide dye self-assemblies and their use as templates for the synthesis of hybrid and supermicroporous nanotubules. *ACS Applied Materials & Interfaces* **3**, 4133–4141 (2011).
- [71] Fujimoto, S. *et al.* A simple approach to the Visible-light photoactivation of molecular metal oxides. *Inorganic Chemistry* **56**, 12169–12177 (2017).
- [72] Cameron, J. M. *et al.* Orbital engineering: Photoactivation of an organofunctionalized polyoxotungstate. *Chemistry—A European Journal* **23**, 47–50 (2017).
- [73] Elgrishi, N. *et al.* A practical beginner's guide to cyclic voltammetry. *Journal of Chemical Education* **95**, 197–206 (2018).
- [74] Savéant, J. M. Elements of molecular and biomolecular electrochemistry. *Wiley-VCH, New Jersey* (2006).
- [75] Shin, I. S. *et al.* Efficient fluorescence "turn-on" sensing of dissolved oxygen by electrochemical switching. *Analytical Chemistry* **84**, 9163–9168 (2012).
- [76] Lee, S. K. *et al.* Electrochemistry, spectroscopy and electrogenerated chemiluminescence of perylene, terylene, and quaterylene diimides in aprotic solution. *Journal of the American Chemical Society* **121**, 3513–3520 (1999).
- [77] Agustin, D., Dallery, J., Coelho, C., Proust, A. & Thouvenot, R. Synthesis, characterization and study of the chromogenic properties of the hybrid polyox-

- ometalates $[\text{PW}_{11}\text{O}_{39}(\text{SiR})_2\text{O}]^{3-}$ (R=Et, $(\text{CH}_2)_n\text{CH}=\text{CH}_2$ (n= 0, 1, 4), $\text{CH}_2\text{CH}_2\text{SiEt}_3$, $\text{CH}_2\text{CH}_2\text{SiMe}_2\text{Ph}$). *Journal of Organometallic Chemistry* **692**, 746–754 (2007).
- [78] Boujtita, M., Boixel, J., Blart, E., Mayer, C. R. & Odobel, F. Redox properties of hybrid Dawson type polyoxometalates disubstituted with organo-silyl or organo-phosphoryl moieties. *Polyhedron* **27**, 688–692 (2008).
- [79] Würthner, F. Perylene bisimide dyes as versatile building blocks for functional supramolecular architectures. *Chemical Communications* 1564–1579 (2004).
- [80] Ford, W. E. Photochemistry of 3, 4, 9, 10-perylenetetracarboxylic dianhydride dyes: visible absorption and fluorescence of the di(glycyl)imide derivative monomer and dimer in basic aqueous solutions. *Journal of Photochemistry* **37**, 189–204 (1987).
- [81] Zhang, W., Gacs, J., Arends, I. W. & Hollmann, F. Selective photooxidation reactions using water-soluble anthraquinone photocatalysts. *ChemCatChem* **9**, 3821–3826 (2017).
- [82] Shen, Q. *et al.* NMR study on solubility of benzyl alcohol and its transfer free energy from D_2O to cationic micelle. *Chinese Journal of Chemistry* **15**, 405–409 (1997).
- [83] Maldotti, A., Molinari, A. *et al.* Design of heterogeneous photocatalysts based on metal oxides to control the selectivity of chemical reactions. *Top. Curr. Chem* **303**, 185–216 (2011).
- [84] Graham, C. R. & Finke, R. G. The classic Wells-Dawson polyoxometalate, $\text{K}_6[\alpha\text{-P}_2\text{W}_{18}\text{O}_{62}] \cdot 14\text{H}_2\text{O}$. Answering an 88 year-old question: What is its preferred, optimum synthesis? *Inorganic Chemistry* **47**, 3679–3686 (2008).